Available online at www.sciencedirect.com
ScienceDirect
Journal of Computational Physics 227 (2008) 5535–5560
JOURNAL OF COMPUTATIONAL PHYSICS
www.elsevier.com/locate/jcp

Quasi-equilibrium grid algorithm: Geometric construction for model reduction

Eliodoro Chiavazzo *, Iliya V. Karlin

Aerothermochemistry and Combustion Systems Laboratory (LAV), ETHZ CH-8092 Zurich, Switzerland

Received 17 April 2007; received in revised form 19 December 2007; accepted 4 February 2008
Available online 16 February 2008

Abstract

The method of invariant grid (MIG) is an iterative procedure for model reduction in chemical kinetics which is based on the notion of Slow Invariant Manifold (SIM) [A.N. Gorban, I.V. Karlin, Method of invariant manifold for chemical kinetics, Chem. Eng. Sci. 58 (2003) 4751–4768; E. Chiavazzo, A.N. Gorban, I.V. Karlin, Comparison of invariant manifolds for model reduction in chemical kinetics, Commun. Comput. Phys. 2(5) (2007) 964–992; A.N. Gorban, I.V. Karlin, A.Y. Zinovyev, Invariant grids for reaction kinetics, Physica A 333 (2004) 106–154; A.N. Gorban, I.V. Karlin, Invariant Manifolds for Physical and Chemical Kinetics, Lecture Notes Physics 660, Springer, Berlin Heidelberg, 2005, doi: 10.1007/b98103]. Important role, in that method, is played by the initial grid which, once refined, gives a description of the invariant manifold: the invariant grid. A convenient way to get a first approximation of the SIM is given by the spectral quasi-equilibrium manifold (SQEM) [A.N. Gorban, I.V. Karlin, Method of invariant manifold for chemical kinetics, Chem. Eng. Sci. 58 (2003) 4751–4768; E. Chiavazzo, A.N. Gorban, I.V. Karlin, Comparison of invariant manifolds for model reduction in chemical kinetics, Commun. Comput. Phys. 2(5) (2007) 964–992]. In the present paper, a flexible numerical method to construct the discrete analog of a quasi-equilibrium manifold, in any dimension, is presented. That object is named quasi-equilibrium grid (QEG), while the procedure quasi-equilibrium grid algorithm (QEGA). Extensions of the QEM notion are also suggested. The QEGA is a numerical tool which can be used to find a grid-based approximation for the locus of minima of a convex function under some linear constraints. The method is validated by construction of one and two-dimensional grids for a model of hydrogen oxidation reaction.

Keywords: Chemical kinetics; Model reduction; Invariant manifold; Entropy; Non-linear dynamics; Lagrange multipliers method; Variational problem

1. Introduction

Relaxation of complex systems is often characterized by a fast dynamics during a short initial stage, while the remaining period lasts much longer and it evolves along low-dimensional surfaces in the phase space known as slow invariant manifolds (SIM). In that scenario, a simplified macroscopic description of a complex

* Corresponding author.
E-mail addresses: chiavazzo@lav.mavt.ethz.ch (E. Chiavazzo), karlin@lav.mavt.ethz.ch (I.V. Karlin).

0021-9991/$ - see front matter © 2008 Elsevier Inc. All rights reserved.
doi:10.1016/j.jcp.2008.02.006

system can be attained by extracting only the slow dynamics and neglecting the fast one. For this reason, much effort was spent to develop model reduction methods (the method of invariant grid (MIG) [9–12], the intrinsic low-dimensional manifold method (ILDM) [25,26,39], the computational singular perturbation method (CSP) [27–29], the equation-free approach [30], the singular PDEs method [32], the iterative procedure in [41], etc.) based on the notion of SIM. The introduction of a convex Lyapunov function G, whenever the complex system supports such a function, also proves to be very helpful in model reduction [12,18]. This is, in particular, the case of chemical reactions in a closed system addressed in this paper. Indeed, it was shown that, through a G function, good approximations of the SIM can be found (e.g. by constructing the spectral quasi-equilibrium manifold – SQEM – or the symmetric entropic intrinsic low-dimensional manifold – SEILDM – [9,10]) and refined by efficient MIG iterations. Moreover, it has been shown that the notion of QEM is also useful in different fields. For example, it was used in the implementation of Lattice Boltzmann schemes [16,17]. Construction of a QEM is addressed by minimization of G under linear constraints. Hence, the approach of the Lagrange multipliers method can be used. More details about the Lagrange multipliers method can be found in the classical work of Rockafellar [5]. In the present paper, the notion of quasi-equilibrium grid (QEG) is introduced, as a discrete analog of QEM, and a constructive algorithm is developed. The procedure suggested proves to be a flexible tool for constructing approximations of SIM.

2. Paper organization

The paper is organized as follows. In Section 3, basic notions are outlined: in particular, the general equations of dissipative reaction kinetics are reviewed in the notations which are used throughout the paper. At the end of that Section, the method of invariant grid (MIG), the notion and properties of thermodynamic projector are briefly discussed (Section 3.2). In Section 4, the QEM definition and its geometrical interpretation are reviewed, while in Section 5 the 1D quasi-equilibrium grid algorithm is presented. That algorithm is also illustrated, by means of an example, in Section 6. The extension of that algorithm to multi-dimensional grids is developed in Section 7. In particular, two possible extension strategies are analyzed: the *straightforward extension* (Section 7.1) and, following the general idea given in [11], the *flag extension* (Section 7.2). The notions of *Guided-QEG* and *symmetric entropic guided-QEG* are introduced in Section 7.3. Further details about the construction of a quasi-equilibrium grid are given in Section 8. An illustrative example, in Section 9, shows how those extension techniques work in practice. In order to find out how accurate is their SIM description, they are also compared on the basis of the invariance defect (Section 9.3). A general discussion about the QEGA is given in Section 10. Finally, results are summarized in Section 11.

3. Theoretical background

3.1. Dissipative reaction kinetics

In a closed system with n chemical species $A_1, \ldots, A_n$, participating in a complex reaction, a generic reversible reaction step can be written as a stoichiometric equation:

$$\alpha_{s1}A_1 + \cdots + \alpha_{sn}A_n \rightleftharpoons \beta_{s1}A_1 + \cdots + \beta_{sn}A_n, \tag{1}$$

where s is the reaction index, $s = 1, \ldots, r$ (r steps in total), and the integers α_{si} and β_{si} are stoichiometric coefficients of the step s. For each reaction step, we can introduce n-component vectors $\boldsymbol{\alpha}_s$ and $\boldsymbol{\beta}_s$, with components α_{si} and β_{si}, and the stoichiometric vector $\boldsymbol{\gamma}_s = \boldsymbol{\beta}_s - \boldsymbol{\alpha}_s$. For every A_i, the *extensive variable* N_i describes the number of particles of that species. If V is the volume, then the concentration of A_i is $c_i = N_i/V$. Dynamics of the species concentration according to the stoichiometric mechanism (1) reads:

$$\dot{\boldsymbol{N}} = V\boldsymbol{J}(\boldsymbol{c}), \quad \boldsymbol{J}(\boldsymbol{c}) = \sum_{s=1}^{r} \boldsymbol{\gamma}_s W_s(\boldsymbol{c}), \tag{2}$$

where dot denotes the time derivative and $W_s(\boldsymbol{c})$ is the reaction rate function of the step s. In particular, the polynomial form of the reaction rate function is provided by *the mass action law*:

$$W_s(\boldsymbol{c}) = W_s^+(\boldsymbol{c}) - W_s^-(\boldsymbol{c}) = k_s^+(T)\prod_{i=1}^{n} c_i^{\alpha_i} - k_s^-(T)\prod_{i=1}^{n} c_i^{\beta_i}, \tag{3}$$

where $k_s^+(T)$ and $k_s^-(T)$ are the constants of the direct and of the inverse reactions rates of the step s, respectively. The most popular form of their dependence is given by the Arrhenius equation:

$$k_s^{\pm}(T) = a_s^{\pm} T^{b_s^{\pm}} \exp(S_s^{\pm}/k_B)\exp(-H_s^{\pm}/k_B T).$$

In the latter equation, $a_s^{\pm}$, $b_s^{\pm}$ are constants and $H_s^{\pm}$, $S_s^{\pm}$ activation enthalpies and entropies, respectively. The rate constants are not independent. Indeed, the *principle of detailed balance* gives a relation between these quantities:

$$W_s^+(\boldsymbol{c}^{\mathrm{eq}}) = W_s^-(\boldsymbol{c}^{\mathrm{eq}}) \quad \forall s = 1,\ldots,r, \tag{4}$$

where the positive vector $\boldsymbol{c}^{\mathrm{eq}}(T)$ is the equilibrium of the system (2). In order to obtain a closed system of equations, one should supply an additional condition for the volume V. For an isolated system the extra-equations are $U, V = \mathrm{const}$ (where U is the internal energy), for an isochoric isothermal system we get $V, T = \mathrm{const}$, and so forth. For example, Eq. (2) in the latter case simply takes the form:

$$\dot{\boldsymbol{c}} = \sum_{s=1}^{r} \gamma_s W_s(\boldsymbol{c}) = \boldsymbol{J}(\boldsymbol{c}). \tag{5}$$

Finally, also other linear constraints, related to the conservation of atoms, must be considered. In general, such conservation laws have the following form:

$$\boldsymbol{D}\boldsymbol{c} = \boldsymbol{const}, \tag{6}$$

where l fixed and linearly independent vectors $\boldsymbol{d}_i$ are the rows of the $l \times n$ matrix $\boldsymbol{D}$, and ***const*** is a constant vector.

3.2. Outline of the method of invariant grid

In this section, we give an outline of the MIG for chemical kinetics. For details see Refs. [9–12,18].

3.2.1. Thermodynamic potential

If we turn our attention to perfectly stirred closed chemically active mixtures, then dissipative properties of such systems can be characterized with a thermodynamic potential which is the Lyapunov function of (2) [6,31]. That function implements the second law of thermodynamics: it means that during the concentration evolution in time, from the initial condition to the equilibrium state, the Lyapunov function must decrease monotonically. Therefore, if $G(\boldsymbol{c})$ is the Lyapunov function, $\boldsymbol{c}^{\mathrm{eq}}$ (equilibrium state) is its point of global minimum in the phase space. A simple example of a function G is given by the free energy of ideal gas in a constant volume and under a constant temperature:

$$G = \sum_{i=1}^{n} c_i[\ln(c_i/c_i^{\mathrm{eq}}) - 1]. \tag{7}$$

when G is known, also its gradient ∇G and the matrix of second derivatives $\boldsymbol{H} = [\partial^2 G/\partial c_i \partial c_j]$ can be evaluated, so that it is possible to introduce the entropic scalar product as follows:

$$\langle \boldsymbol{x}, \boldsymbol{y}\rangle = (\boldsymbol{x}, \boldsymbol{H}\boldsymbol{y}), \tag{8}$$

where the notation (,) is the usual Euclidean scalar product.

3.2.2. The invariance condition

Let $\boldsymbol{\Omega}$ be a general q-dimensional manifold in the concentration space. Let Υ be a subset in the q-dimensional space $\boldsymbol{R}^q$. We assume that $\boldsymbol{\Omega}$ is defined by a function F which maps the points of Υ into the concentration space. In other words, such a manifold $\boldsymbol{\Omega}$ is parametrized by q variables $y_i \in \Upsilon$. Moreover, F is supposed to be sufficiently smooth so that, in any concentration point $\boldsymbol{c} = F(y_1,\ldots,y_q)$ on $\boldsymbol{\Omega}$, the derivatives

$$\boldsymbol{f}_i = \frac{\partial F}{\partial y_i}, \quad i = 1, \ldots, q \tag{9}$$

can be evaluated. For each point $\boldsymbol{c}$ of $\boldsymbol{\Omega}$, the tangent space T is given by the linear sub-space spanned by vectors $\boldsymbol{f}_i$: $T = \mathrm{Lin}\{\boldsymbol{f}_i\}$. In that case, a projector may be introduced at the point $\boldsymbol{c}$. Let $\boldsymbol{x}$ be a generic n-dimensional vector in the concentration space. A projector $\boldsymbol{P}$ transforms $\boldsymbol{x}$ into another n-dimensional vector $\boldsymbol{P}\boldsymbol{x} \in T$ and fulfills the following property: $\boldsymbol{P}(\boldsymbol{P}\boldsymbol{x}) = \boldsymbol{P}\boldsymbol{x}$. Furthermore, we require that the image of $\boldsymbol{P}$ spans the tangent space T ($\mathrm{im}(\boldsymbol{P}) = T$). In general, a manifold $\boldsymbol{\Omega}$ is (positively) invariant with respect to the system (2) when:

$$\boldsymbol{c}(0) \in \boldsymbol{\Omega} \Rightarrow \boldsymbol{c}(t) \in \boldsymbol{\Omega} \quad \forall t \geqslant 0. \tag{10}$$

Alternatively, $\boldsymbol{\Omega}$ is an invariant manifold (with respect to (2)) if and only if the invariance condition holds:

$$[1 - \boldsymbol{P}]\boldsymbol{J}(\boldsymbol{c}) = 0 \quad \forall \boldsymbol{c} \in \boldsymbol{\Omega}. \tag{11}$$

when the manifold $\boldsymbol{\Omega}$ is not invariant, it is not able to satisfy the invariance condition so that:

$$\exists \boldsymbol{c}_0 \in \boldsymbol{\Omega} : \Delta_0 = [1 - \boldsymbol{P}]\boldsymbol{J}(\boldsymbol{c}_0) \neq 0, \tag{12}$$

where Δ_0 is the defect of invariance.

Remark. A projector $\boldsymbol{P}$ is defined at the points of a smooth q-dimensional manifold $\boldsymbol{\Omega}$. Such a manifold may (or may not) be invariant. Notice that, for constructing a projector $\boldsymbol{P}$ at a given point $\boldsymbol{c}^* \in \boldsymbol{\Omega}$, the tangent vectors (9) are needed. In general, evaluation of those vectors does not require a global map F: a local one can be safely used for that scope (only derivatives of F at $\boldsymbol{c}^*$ are requested). In that sense, the invariance defect (12) $\Delta(\boldsymbol{c}^*)$ can be considered a local quantity.

3.2.3. Projectors and dissipation inequality

Let us now discuss further the projector appearing in the invariance equation. It is an operator which for each point $\boldsymbol{c} \in \boldsymbol{\Omega}$ projects the vector $\boldsymbol{J}(\boldsymbol{c})$ onto the tangent subspace of the manifold producing, in this way, the induced vector field $\boldsymbol{P}\boldsymbol{J}(\boldsymbol{c})$ of the reduced dynamics. In general, condition (11) does not require any special constraint for $\boldsymbol{P}$. However, the thermodynamic properties of the kinetic equations (2) define the projector unambiguously [9,12,18,36]. To this end, let us define a differential of G, that is, a linear functional:

$$DG(\boldsymbol{x}) = (\nabla G(\boldsymbol{c}), \boldsymbol{x}). \tag{13}$$

A special class of projectors is the thermodynamic one. If a projector belongs to this class then the induced vector field respects the dissipation inequality:

$$DG(\boldsymbol{P}\boldsymbol{J}) \leqslant 0 \quad \forall \boldsymbol{c} \in \boldsymbol{\Omega}. \tag{14}$$

It has been shown that a projector $\boldsymbol{P}$ respects condition (14) if and only if [18]:

$$\ker \boldsymbol{P} \subseteq \ker DG \quad \forall \boldsymbol{c} \in \boldsymbol{\Omega}, \tag{15}$$

where ker denotes the null-space of an operator.

3.2.4. Construction of thermodynamic projector

For solving the invariance equation (11) by iterations starting from an initial guess for the invariant manifold, a projector must be specified on each iteration. Here, we remind the way to construct the thermodynamic projector which is used in the MIG procedure [9]. This projector depends on the point $\boldsymbol{c}$ of a manifold $\boldsymbol{\Omega}$ and on the tangent space to $\boldsymbol{\Omega}$ at that point. In the sequel, we are dealing with grid approximation of a q-dimensional SIM. Let $\mathcal{G}$ be a discrete subset of a q-dimensional variables space $\boldsymbol{R}^q$ and let $F|_{\mathcal{G}}$ be a mapping of $\mathcal{G}$ into the concentration space. If we select an approximation procedure to restore the smooth map F from the discrete map $F|_{\mathcal{G}}$ (we need a small part of F, derivatives of F in the grid points only), then the derivatives $\boldsymbol{f}_i = \partial F/\partial y_i$ are available, and for each grid point the tangent space is:

$$T = \mathrm{Lin}\{\boldsymbol{f}_i\}, \quad i = 1, \ldots, q. \tag{16}$$

We assume that one of the points $y \in \mathcal{G}$ maps into the equilibrium, and in other points intersection of the manifold with G levels is transversal (i.e. $(DG)_{F(y)}(x) \neq 0$ for some $x \in T$). Let us consider the subspace $T_0 = (T \cap \ker DG)$. In order to define the thermodynamic projector, it is required, if $T_0 \neq T$, to introduce the vector $\boldsymbol{e}_y$ which satisfies the following conditions:

$$\begin{cases} \boldsymbol{e}_y \in T, \\ \langle \boldsymbol{e}_y, \boldsymbol{x} \rangle = 0 \qquad \forall \boldsymbol{x} \in T_0, \\ DG(\boldsymbol{e}_y) = 1. \end{cases}$$

Let $\boldsymbol{P}_0$ be the orthogonal projector on T_0 with respect to the entropic scalar product (8). Then the thermodynamic projection of a vector $\boldsymbol{x}$ is defined as

$$\begin{cases} T_0 \neq T \Rightarrow \boldsymbol{P}\boldsymbol{x} = \boldsymbol{P}_0\boldsymbol{x} + \boldsymbol{e}_y DG(\boldsymbol{x}) \\ T_0 = T \Rightarrow \boldsymbol{P}\boldsymbol{x} = \boldsymbol{P}_0\boldsymbol{x}. \end{cases} \tag{17}$$

A discussion of pertinent properties of thermodynamic projector is in order.

3.2.5. Discussion about grids and thermodynamic projector

For the sake of clarity, in the present section we want to give some more details about the notions of grid and thermodynamic projector. Let $\mathcal{G}$ be a discrete subset of $\boldsymbol{R}^q$. For every point $y \in \mathcal{G}$, a neighborhood of y, $V_y \subset \mathcal{G}$, can be considered. For regular grids, V_y is a finite set of points which, usually includes the nearest neighbors of y. The notion of the grid becomes useful for our purposes, if grid differential operators on $\mathcal{G}$ are defined. Indeed, once a discrete mapping $F|_{\mathcal{G}}$ of $\mathcal{G}$ into the concentration space is known, there is a need to restore a differentiable map F from it (by approximating, for example, through low-order polynomials) so that the following derivatives:

$$\boldsymbol{f}_i = \left.\frac{\partial F}{\partial y_i}\right|_y = \sum_{\zeta \in V_y} g_i(y,\zeta) F(\zeta) \tag{18}$$

are available in each point y. Here, $g_i(y,\zeta)$ are some coefficients and they are dependent on the chosen approximation. In our calculations, we often make use of second-order polynomials. We assume that (18) can be evaluated in any point of $\mathcal{G}$. We call such grids admissible and, in the sequel, we only deal with admissible grids. In this way, in any grid point y, the subspace, spanned by the q vectors $\{\boldsymbol{f}_i\}$, is the local tangent space T of the grid. Notice that the definition of a grid includes:

(1) A discrete subset $\mathcal{G} \subset R^q$.
(2) A discrete mapping of $\mathcal{G}$ into the concentration space.
(3) The differentiation formulas (18) with given coefficients $g_i(y,\zeta)$.

Moreover, such a grid is defined invariant (with respect to (2)) when, at any point y, the vector field $\boldsymbol{J}(F(y))$ belongs to the tangent space T. For more details see [11]. Here, It is important to stress that the construction of the thermodynamic projector (17) can be carried out, at any grid node (and only there), without a need of a global parametrization. Indeed, the tangent space T can be found at any y, via (18), by only using a local mapping of $V_y \subset \mathcal{G}$ into the phase space. Let us discuss some properties of the thermodynamic projector. Those special features make that operator particularly useful for model reduction. The thermodynamic projector (as well as any other projector appearing in the invariance condition (11)) is characterized by its image and null-space. In general, both those linear subspaces are dependent on the grid point y where $\boldsymbol{P}$ is constructed. Thus, thermodynamic projector is an affine projector. As explained in Section 3.2.2, by construction, the image of such operators spans the tangent subspace T of the grid at y. That is certainly the case for the thermodynamic projector, too. Nevertheless, the null-space of (17) is special. Let the system (2) be stiff. We expect that any solution trajectory in the phase space, after a fast initial transient, is attracted to a low-dimensional manifold $\boldsymbol{\Omega}$ and then it does not leave it any more, moving toward the equilibrium point. $\boldsymbol{\Omega}$ is the slow invariant manifold (SIM) of (2). It is known that a good approximation of those fast motions close to a SIM point $\boldsymbol{c}^*$, are given by the eigenvectors of Jacobian $\boldsymbol{L}(\boldsymbol{c}^*)$ corresponding to eigenvalues with the largest absolute real

part (see, e.g. [25]). Let us consider an invariant grid $\mathcal{G}_{\text{inv}}$. That grid is a discrete analog of the SIM, and its mapped points $F(y)$ in the phase space are expected to be located close to the SIM. The thermodynamic projector is constructed in such a way that, in any invariant grid node $F(y)$, the null space of (17) is "almost" spanned by the fast directions at that point, e.g. the fast eigenvectors of $\boldsymbol{L}(F(y))$. In order to illustrate this important feature, we consider the following four-step three-component reaction, studied in a more detail in Section 6

$$\begin{cases} 1.\, A \leftrightarrow B, & k_1^+ = 1, \\ 2.\, B \leftrightarrow C, & k_2^+ = 1, \\ 3.\, C \leftrightarrow A, & k_3^+ = 1, \\ 4.\, A + B \leftrightarrow 2C, & k_4^+ = 50. \end{cases} \tag{19}$$

The atom balance takes the form:

$$\boldsymbol{D}\boldsymbol{c} = [\,1 \quad 1 \quad 1\,] \begin{bmatrix} c_A \\ c_B \\ c_C \end{bmatrix} = 1 \tag{20}$$

and the equilibrium point is chosen as: $c_A^{\text{eq}} = 0.1$, $c_B^{\text{eq}} = 0.5$, $c_C^{\text{eq}} = 0.4$. Because of the constraint (20), the system is effectively two-dimensional. As shown in Fig. 1a, any solution trajectory, after a rapid initial dynamics, is attracted to a 1D curve and along it reaches the equilibrium point. The system is closed and the reaction (19) takes place under constant volume and temperature, so that here the Lyapunov function is (7). A one-dimensional invariant grid, parametrized by the concentration c_B, was considered (diamonds in Fig. 1a). In any grid node, the Jacobian matrix $\boldsymbol{L}$ was evaluated. Through spectral decomposition of $\boldsymbol{L}$, it was possible to estimate the fast direction $\boldsymbol{a}_{\text{f}}$ (eigenvector corresponding to the eigenvalue with the largest absolute value) and the slow direction $\boldsymbol{a}_{\text{s}}$ (eigenvector corresponding to the eigenvalue with the smallest absolute value). Both eigenvectors were projected, by means of the thermodynamic projector (17), at each node. In Fig. 1b, the Euclidean norm of those projections $\|\boldsymbol{P}\boldsymbol{a}_i\|$ is plotted versus the grid parameter c_B. The eigenvectors were chosen such that $\|\boldsymbol{a}_{\text{f}}\| = \|\boldsymbol{a}_{\text{s}}\| = 1$. Fig. 2 shows the geometrical meaning and relevance of the thermodynamic projector to the slow–fast decomposition: the fast component of any trajectory "almost" lies in the affine subspace $\boldsymbol{c}^* + \ker \boldsymbol{P}$, where $\boldsymbol{c}^*$ is an invariant grid node while $\ker \boldsymbol{P}$ is the null space of (17) constructed at $\boldsymbol{c}^*$. Note that, although the thermodynamic projector can be constructed whenever an admissible grid is available, the previous result only applies for invariant grids. Therefore, the model reduction problem is split into two subsequent steps:

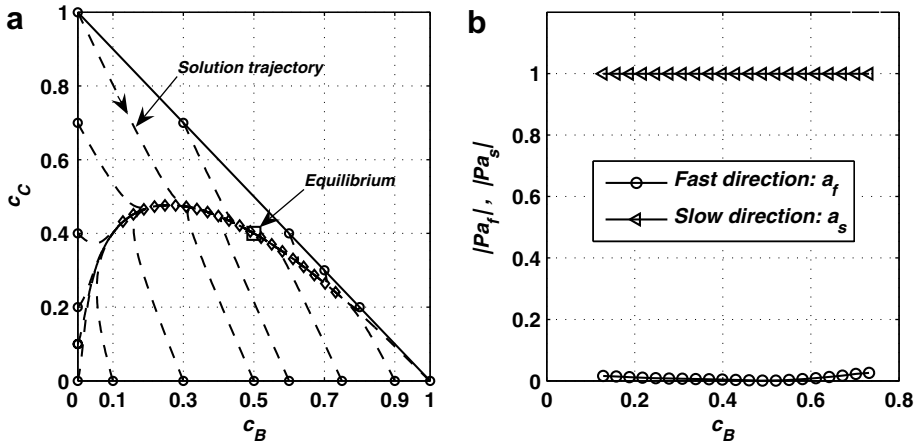

Fig. 1. Four-step three-species mechanism. (a) Solution trajectories in the phase space $c_B - c_C$ (dashed lines). Invariant grid (diamonds). (b) Euclidean norm of the thermodynamic projection of Jacobian eigenvectors at the invariant grid nodes.

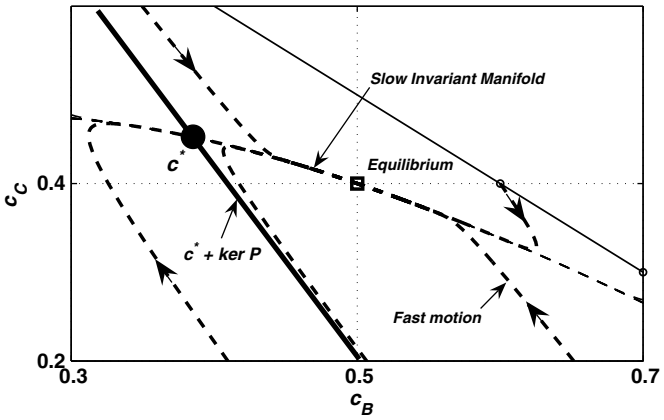

Fig. 2. The fast part of any trajectory lies in the null space (ker $\boldsymbol{P}$) of the thermodynamic projector constructed at the invariant grid nodes.

(1) Construction of the slow invariant manifold.
(2) Reconstruction of the fast subspace.

The thermodynamic projector plays a different role in each of those steps. First, it is used for computing the invariance defect in the iterative procedure of next Sections 3.2.6 and 3.2.7. Second, once the invariant grid (slow subspace) is delivered, also the fast subspace can be reconstructed via null space of (17) at the invariant grid nodes. In that sense, an initial condition for the ODE system (2), off the slow invariant grid $\mathcal{G}_{\text{inv}}$, can be "projected" onto it through the kernel of thermodynamic projector evaluated on $\mathcal{G}_{\text{inv}}$ (see Fig. 2).

3.2.6. Newton method with incomplete linearization

When MIG method is applied, not a manifold is searched as a solution, but a set of points $\mathcal{G}_{\text{inv}}$ whose defect of invariance is sufficiently small. MIG is an iterative procedure, that is, at the beginning, only an initial approximation $\mathcal{G}_0$ is available. In general, $\mathcal{G}_0$ does not respect the invariance condition (11) satisfactorily so that (12) holds. For this reason the position of $\boldsymbol{c}_0 \in \mathcal{G}_0$ must be refined. We can think to correct its location to get a new point, $\boldsymbol{c}_0 + \delta\boldsymbol{c}$, with a smaller defect of invariance, $\boldsymbol{\Delta} = [1 - \boldsymbol{P}]\boldsymbol{J}(\boldsymbol{c}_0 + \delta\boldsymbol{c})$. If the initial node is "not far" from the invariant manifold, a reasonable way to get the node correction $\delta\boldsymbol{c}$ is to solve the linearized invariance equation where the vector field $\boldsymbol{J}$ is expanded to first order and the projector $\boldsymbol{P}$ to zeroth order:

$$[1 - \boldsymbol{P}][\boldsymbol{J}(\boldsymbol{c}) + \boldsymbol{L}(\boldsymbol{c})\delta\boldsymbol{c}] = 0. \tag{21}$$

Here, $\boldsymbol{L}$ is the matrix of first derivatives of $\boldsymbol{J}$ (Jacobian matrix). The Newton method with incomplete linearization consists of Eq. (21) supplied by the extra condition [18]:

$$\boldsymbol{P}\delta\boldsymbol{c} = 0. \tag{22}$$

The additional condition (22) and the atom constraints (6) automatically can be taken into account by choosing a basis $\{\boldsymbol{b}_i\}$ in the subspace $\boldsymbol{S} = (\ker \boldsymbol{P} \cap \ker \boldsymbol{D})$. Let $h = dim(\boldsymbol{S})$, then the correction can be cast in the form $\delta\boldsymbol{c} = \sum_{i=1}^{h} \delta_i \boldsymbol{b}_i$, so that the linearized invariance equation (21) becomes the linear algebraic system in terms of δ_i:

$$\sum_{i=1}^{h} \delta_i((1 - \boldsymbol{P})\boldsymbol{L}\boldsymbol{b}_i, \boldsymbol{b}_k) = -((1 - \boldsymbol{P})\boldsymbol{J}, \boldsymbol{b}_k), \quad k = 1, \ldots, h. \tag{23}$$

Remark. Here, without a loss of generality, the usual scalar product (,) was used to get the components of the left-hand side of (21) in the basis vectors $\{\boldsymbol{b}_i\}$. However, a different scalar product can be also used.

In the case of the thermodynamic projector, it proves convenient to choose the basis $\{\boldsymbol{b}_i\}$ orthonormal with respect to the entropic scalar product (8) and write Eq. (23) as

$$\sum_{i=1}^{h} \delta_i \langle (1-\boldsymbol{P})\boldsymbol{L}\boldsymbol{b}_i, \boldsymbol{b}_k \rangle = -\langle (1-\boldsymbol{P})\boldsymbol{J}, \boldsymbol{b}_k \rangle, \quad k = 1, \ldots, h. \tag{24}$$

The projector (17) is "almost $\langle , \rangle$-orthogonal", that is, $\langle \mathrm{im}\boldsymbol{P}, \ker \boldsymbol{P} \rangle \cong 0$ close to the SIM. Because of that special feature, Eq. (24) can be approximated and simplified as follows:

$$\sum_{i=1}^{h} \delta_i \langle \boldsymbol{L}\boldsymbol{b}_i, \boldsymbol{b}_k \rangle = -\langle \boldsymbol{J}, \boldsymbol{b}_k \rangle, \quad k = 1, \ldots, h. \tag{25}$$

Note that, in general, an approximation carried out by Eq. (25) leaves a residual defect (12) in the grid nodes which cannot be completely annihilated. Therefore, when a higher accuracy in the SIM description is required, Eq. (23) is recommended.

3.2.7. Relaxation method

An alternative approach to solve Eq. (21) is the *relaxation method*. According to that method the correction is written as $\boldsymbol{c} = \boldsymbol{c}_0 + \tau(\boldsymbol{c})\Delta(\boldsymbol{c})$, and the function $\tau(\boldsymbol{c})$ is obtained from the condition:

$$\langle \Delta, [1-\boldsymbol{P}][\boldsymbol{J} + \tau(\boldsymbol{c})\boldsymbol{L}\Delta] \rangle = 0.$$

Solving with respect to τ, gives:

$$\tau(\boldsymbol{c}) = -\frac{\langle \Delta, \Delta \rangle}{\langle \Delta, \boldsymbol{L}\Delta \rangle}. \tag{26}$$

Eq. (26) shows that the relaxation method is explicit, but since it adjusts the node position acting only along the direction of the defect Δ, typically we expect it to be less efficient in comparison with the Newton method. On the other hand, this method is particularly easy to implement.

Remark. Assume that $\mathcal{G}_{\mathrm{inv}}$ is the invariant grid while $\mathcal{G}_0$ is its initial approximation. Let the thermodynamic projector (17) be constructed on $\mathcal{G}_0$. After the first MIG iteration (e.g. through (23) or (26)) every node of $\mathcal{G}_0$ is refined so that a new grid $\mathcal{G}_1$ is now available. Note that, in order to continue refining, the projector (17) needs to be constructed on the new grid $\mathcal{G}_1$. In general, at any MIG iteration, the grid is refined, consequently the thermodynamic projector, constructed according to (17), also results updated at any iteration.

4. The initial approximation. The quasi-equilibrium manifold

Any iterative procedure needs to be supplied by an initial approximation. Since it plays an important role for both the convergence and efficiency, that approximation must be carefully chosen. It was shown that a reasonable way, for initializing the MIG, is to construct the quasi-equilibrium manifold (QEM) [9,10].

4.1. QEM definition

All trajectories satisfy a set of linear equations (6) which represent the atom conservation. Let us consider q additional linear constraints. Among all the states that fulfill the full set of constraints (atom conservation + extra constraints), we can choose that point which also minimizes the Lyapunov function G of the system we are dealing with. Such a point lies on a manifold that is called the *quasi-equilibrium manifold* (QEM) [12]. Let the ODE system (5) be stiff. In other words, we assume that the Jacobi matrix has eigenvalues with different orders of magnitude. In this case, we expect that a solution trajectory in the phase space, after a short transient, reaches a low-dimensional surface (slow invariant manifold). Indeed, the fast motions are exhausted and they restrain the solution on that surface. If the slow invariant manifold exists, the QEM can be taken as a reasonable approximation of it. For more details about the rationale and applications of QEM, the reader is delegated to [9,12] and Section 10. Let a chemical system have n reactive species. The degrees of freedom of that system are $(n-l)$ because of the atom balances (6). If $q < (n-l)$ is the dimension of the QEM, then the macroscopic variables for its description are $\xi_1, \ldots, \xi_q$ so that: $(\boldsymbol{m}_1, \boldsymbol{c}) = \xi_1, \ldots, (\boldsymbol{m}_q, \boldsymbol{c}) = \xi_q$. From a mathematical standpoint, the solution of a variational problem:

$$\begin{cases} G \to \min, \\ (\boldsymbol{m}_i, \boldsymbol{c}) = \xi_i \quad \forall i = 1, \ldots, q, \\ \boldsymbol{D}\boldsymbol{c} = \boldsymbol{const}, \end{cases} \tag{27}$$

represents the QEM corresponding to the vector set $\{\boldsymbol{m}_i\}$. Note that there is no general recipe for choosing the set $\{\boldsymbol{m}_i\}$. Nevertheless, in this paper we work out some suggestions for this (see, e.g. the SQEG below or the GQEG construction in Section 7.3). Similarly, the dimension q belongs to the input data for the problem (27). Now, we want to stress the geometry behind (27) because it will be extensively exploited in the sequel. The geometric interpretation of a QEM is illustrated in Fig. 3 for a two-dimensional phase space (c_{A_i}, c_{A_j}). Let us consider the points where G level curves (convex curves in Fig. 3a and b) are cut by the QE-manifolds (bold curves): in those points the inclination of the tangent to the G-level curves is constant. Different QEM can be obtained by choosing different vector sets $\{\boldsymbol{m}_i\}$. A special choice is done when $\{\boldsymbol{m}_1, \ldots, \boldsymbol{m}_q\}$ are the q left eigenvectors of the Jacobi matrix $\boldsymbol{L}(\boldsymbol{c}^{\mathrm{eq}})$ corresponding to the q eigenvalues with smallest absolute value. In that particular case, solution of (27) has its own name: *spectral quasi-equilibrium manifold* (SQEM) [9,10].

4.2. Quasi-equilibrium manifold in practice

The minimization problem (27) can be solved by the method of Lagrange multipliers [5]. However, it is also known that, when the number of constraints and variables increases, then that method may become computationally intensive (see also [20]). In the sequel, a new procedure to overcome that issue is presented. An algorithm (*quasi-equilibrium grid algorithm*), which can be implemented in order to get a discrete analog of a QEM in any dimension, is developed. This is achieved by investigating further the QEM geometrical construction.

5. 1D quasi-equilibrium grid (QEG) construction

First, let us consider a one-dimensional quasi-equilibrium manifold, that is, the set $\{\boldsymbol{m}_i\}$ consists of one vector $\boldsymbol{m}$. Let us assume that a node $\boldsymbol{c}_0$ belongs to that manifold. One may now look for a new node $\boldsymbol{c}_1$ belonging to the quasi-equilibrium manifold. In general, the node $\boldsymbol{c}_1$ can be obtained from $\boldsymbol{c}_0$ by shifting: $\boldsymbol{c}_1 = \boldsymbol{c}_0 + \hat{\delta}\boldsymbol{c}_0$. This idea is applicable whenever a QEM-node $\boldsymbol{c}_n$ is known and a new one $\boldsymbol{c}_{n+1}$ must be found (see Fig. 4):

$$\boldsymbol{c}_{n+1} = \boldsymbol{c}_n + \hat{\delta}\boldsymbol{c}_n. \tag{28}$$

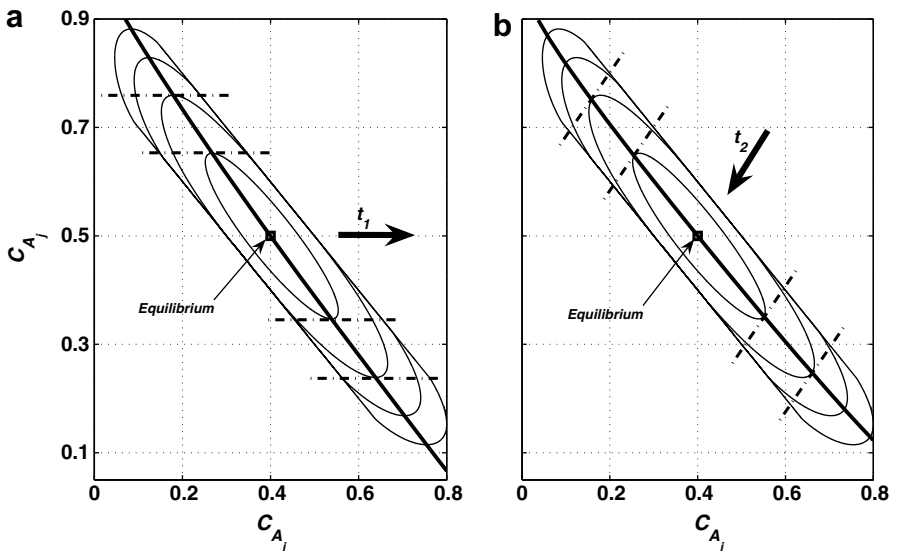

Fig. 3. Quasi-equilibrium manifold: the geometrical interpretation. Two different QE-manifolds (bold lines in (a) and (b)) corresponding to two different sets of linear constraints in the problem (27).

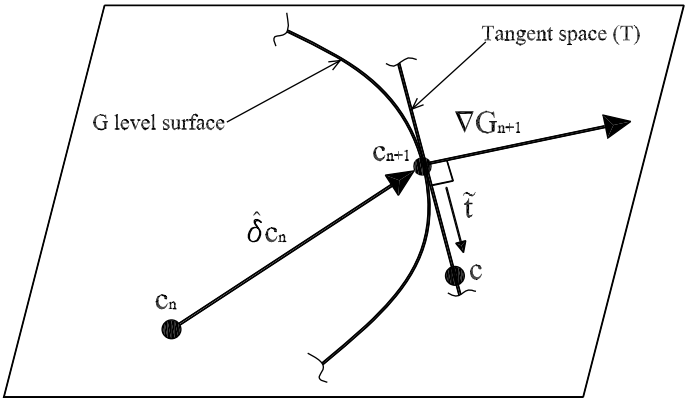

Fig. 4. Quasi-equilibrium grid: the basic idea.

First of all, any node $\boldsymbol{c}_n$ has to fulfill the constraint of atom conservation (6). Let $\{\boldsymbol{\rho}_i\}$ be a basis in the null space of matrix $\boldsymbol{D}$. A convenient way to take conservation conditions (6) automatically into account is to express any shift $\hat{\delta}\boldsymbol{c}_n$ as a linear combination of vectors $\boldsymbol{\rho}_i$:

$$\hat{\delta}\boldsymbol{c}_n = \sum_{i=1}^{z} \mu_i \boldsymbol{\rho}_i, \tag{29}$$

where $z = n - l$ is the dimension of the basis $\{\boldsymbol{\rho}_i\}$. By referring to Fig. 4, let us now discuss further the tangent space T to the G level surface in any quasi-equilibrium point $\boldsymbol{c}_{n+1}$. The space T geometrically represents the linear constraints of the problem (27). Therefore, any point $\boldsymbol{c}$ of T satisfies that constraint, but only $\boldsymbol{c}_{n+1}$ minimizes G function. The line l passing from $\boldsymbol{c}_{n+1}$ and $\boldsymbol{c}$ has the parametric form $\boldsymbol{c} = \varphi\tilde{\boldsymbol{t}} + \boldsymbol{c}_{n+1}$, where $\tilde{\boldsymbol{t}}$ is a vector of T spanning l while φ is a parameter. In general, the linear constraints of the problem (27) can be also written as:

$$\begin{cases} (\boldsymbol{m}, \boldsymbol{c}) = \varphi(\boldsymbol{m}, \tilde{\boldsymbol{t}}) + (\boldsymbol{m}, \boldsymbol{c}_{n+1}) \Rightarrow (\boldsymbol{m}, \tilde{\boldsymbol{t}}) = 0 \quad \forall \tilde{\boldsymbol{t}}, \\ (\boldsymbol{d}_i, \boldsymbol{c}) = \varphi(\boldsymbol{d}_i, \tilde{\boldsymbol{t}}) + (\boldsymbol{d}_i, \boldsymbol{c}_{n+1}) \Rightarrow (\boldsymbol{d}_i, \tilde{\boldsymbol{t}}) = 0 \quad \forall \tilde{\boldsymbol{t}}, \end{cases} \tag{30}$$

where $\boldsymbol{m}$ and $\boldsymbol{d}_i$ are the reduced variable vector ($q = 1$) and the generic row of matrix $\boldsymbol{D}$, respectively. The vector $\tilde{\boldsymbol{t}}$, that respects (30), can always be written as a linear combination of some vectors $\boldsymbol{t}_j$, where $\{\boldsymbol{t}_j\}$ denotes a basis in the null space of that matrix $\boldsymbol{E}$, whose first row is given by $\boldsymbol{m}$ and the rest by the rows of $\boldsymbol{D}$:

$$\boldsymbol{E} = \begin{bmatrix} \boldsymbol{m} \\ \boldsymbol{D} \end{bmatrix}. \tag{31}$$

Note that the dimension of $\{\boldsymbol{t}_j\}$ is $z - 1$. The *quasi-equilibrium requirement* simply becomes the orthogonality condition:

$$(\nabla G(\boldsymbol{c}_{n+1}), \tilde{\boldsymbol{t}}) = 0 \quad \forall \tilde{\boldsymbol{t}} \in T, \tag{32}$$

which also means:

$$(\nabla G(\boldsymbol{c}_{n+1}), \boldsymbol{t}_j) = 0 \quad \forall j = 1, \ldots, z-1. \tag{33}$$

The quasi-equilibrium grid algorithm is based on the system (33) and two further assumptions. First, we assume that the known node $\boldsymbol{c}_n$ is close to the QEM, although it does not necessarily belong to the QEM. Secondly, let the vector $\hat{\delta}\boldsymbol{c}_n$ be small enough, so that the gradient $\nabla G(\boldsymbol{c}_{n+1})$ can be approximated to first order:

$$\nabla G(\boldsymbol{c}_{n+1}) \cong \nabla G(\boldsymbol{c}_n) + \boldsymbol{H}(\boldsymbol{c}_n)\hat{\delta}\boldsymbol{c}_n, \tag{34}$$

where $\boldsymbol{H}(\boldsymbol{c}_n) = \left[\frac{\partial^2 G}{\partial c_i \partial c_j}\right]$ denotes the matrix of second derivatives of the function G evaluated at the point $\boldsymbol{c}_n$. Upon substitution of Eqs. (34) and (29) in (33), we obtain:

$$\sum_{i=1}^{z}(\boldsymbol{t}_j, \boldsymbol{H}(\boldsymbol{c}_n)\boldsymbol{\rho}_i)\mu_i = -(\boldsymbol{t}_j, \nabla G(\boldsymbol{c}_n)) \quad \forall j = 1, \ldots, z-1. \tag{35}$$

By using the entropic scalar product (8), Eq. (35) can be cast into the form:

$$\sum_{i=1}^{z}\langle \boldsymbol{t}_j, \boldsymbol{\rho}_i\rangle \mu_i = -(\boldsymbol{t}_j, \nabla G(\boldsymbol{c}_n)) \quad \forall j = 1, \ldots, z-1. \tag{36}$$

Both the matrix $\boldsymbol{H}$ and the gradient ∇G are calculated at the known node $\boldsymbol{c}_n$. Note that the right-hand side of (36) vanishes if the node $\boldsymbol{c}_n$ belongs to the QEM. The node collection, subsequently evaluated through (36), will be called a *quasi-equilibrium grid* (QEG).

5.1. Closure through the spacing condition

Note, however, that the system (36) is not closed (z unknowns μ_i, but $z-1$ equations) because it lacks a further information about the grid spacing. A reasonable closure for that system can be achieved by fixing the grid spacing (e.g. in Euclidean sense):

$$\begin{cases} \sum_{i=1}^{z}\langle \boldsymbol{t}_j, \boldsymbol{\rho}_i\rangle \mu_i = -(\boldsymbol{t}_j, \nabla G(\boldsymbol{c}_n)) \quad \forall j = 1, \ldots, z-1, \\ \|\hat{\delta}\boldsymbol{c}_n\| = \varepsilon, \end{cases} \tag{37}$$

where ε is a given number and $\|\hat{\delta}\boldsymbol{c}_n\|$ represents Euclidean norm of the vector $\hat{\delta}\boldsymbol{c}_n$. The smaller ε is chosen, the more accurate the expression (34) is. As it will be shown below, for small ε the QEG lies very close to the correspondent quasi-equilibrium manifold. Additional condition makes (37) a non-linear algebraic system. A way to solve it will be now discussed. The idea is to find the general solution of the linear system (36), and then to choose the one which also fulfills the non-linear condition in (37). Let the basis $\{\boldsymbol{\rho}_i\}$ be orthonormal (in Euclidean sense). That is not crucial, but it proves to be convenient in the following analysis. Indeed, the non-linear system (37) now is cast in the following form:

$$\begin{cases} \sum_{i=1}^{z}\langle \boldsymbol{t}_j, \boldsymbol{\rho}_i\rangle \mu_i = -(\boldsymbol{t}_j, \nabla G(\boldsymbol{c}_n)) \quad \forall j = 1, \ldots, z-1, \\ \sum_{i=1}^{z}\mu_i^2 = \varepsilon^2. \end{cases} \tag{38}$$

A general solution of (36) can always be written as:

$$\begin{bmatrix} \mu_1 \\ \vdots \\ \mu_z \end{bmatrix} = w \begin{bmatrix} v_1 \\ \vdots \\ v_z \end{bmatrix} + \begin{bmatrix} p_1 \\ \vdots \\ p_z \end{bmatrix}, \tag{39}$$

where w is a given parameter, while $\boldsymbol{v} = [v_1, \ldots, v_z]^{\mathrm{T}}$ and $\boldsymbol{p} = [p_1, \ldots, p_z]^{\mathrm{T}}$ are the solution of the homogeneous problem and a special solution of (36), respectively. Without any restriction, we assume $(\boldsymbol{v}, \boldsymbol{v}) = 1$. Once $\boldsymbol{v}$ and $\boldsymbol{p}$ are known, the non-linear condition in (38) can be written, in terms of w, as

$$w^2 + 2(\boldsymbol{v}, \boldsymbol{p})w + (\boldsymbol{p}, \boldsymbol{p}) - \varepsilon^2 = 0. \tag{40}$$

If the solvability condition is satisfied,

$$(\boldsymbol{v}, \boldsymbol{p})^2 - (\boldsymbol{p}, \boldsymbol{p}) + \varepsilon^2 s > 0, \tag{41}$$

then the two real valued solutions of (40) (w^{I}, w^{II}), upon substitution into (39), give two possible sets $[\mu_1, \ldots, \mu_z]$. Therefore, by using (28) and (29), two new nodes, $\boldsymbol{c}_{n+1}^{\mathrm{I}}$ and $\boldsymbol{c}_{n+1}^{\mathrm{II}}$ (both close to the quasi-equilibrium manifold) can be evaluated from the previous node $\boldsymbol{c}_n$ (see Fig. 5). A criterion, able to choose between these two solutions, depends on the phase space zone where the grid needs to be constructed. This idea will be clarified in Section 8. Usually, the equilibrium point is supposed to be a good starting node for the QEG procedure: $\boldsymbol{c}_0 = \boldsymbol{c}^{\mathrm{eq}}$.

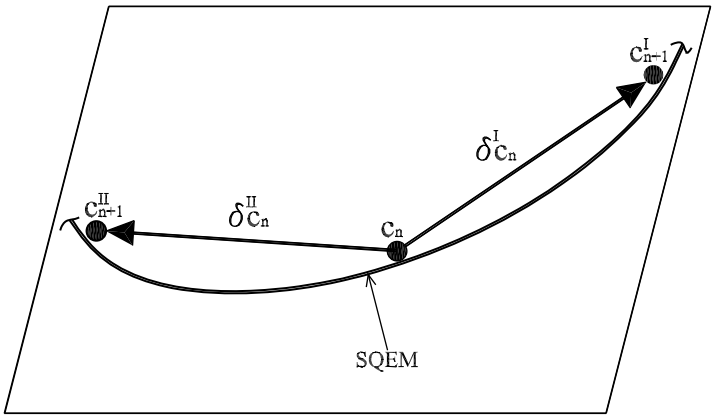

Fig. 5. Two solutions for the 1D QEG algorithm.

Remark. The QEG-equations (36) can be generalized as follows:

$$\sum_{i=1}^{z}\langle \boldsymbol{t}_j, \boldsymbol{\rho}_i\rangle \mu_i = -\eta(\boldsymbol{t}_j, \nabla G(\boldsymbol{c}_n)) \quad \forall j = 1,\ldots,z-1, \tag{42}$$

where η is a parameter $0 \leqslant \eta \leqslant 1$. When $\eta = 1$, (36) is recovered. On the other hand, if the QEG-nodes are close to the QEM, then the non-homogeneous terms can be neglected (they vanish on the QEM). Therefore, a reasonable approximation of the system (36) is given when $\eta = 0$. In the latter case, the solvability condition (41) is fulfilled. If $\eta = 1$ and (41) does not hold, that parameter can be chosen in such a way that the solvability condition is satisfied. In the following, if not otherwise stated, it is assumed $\eta = 1$.

6. Example of 1D SQEG algorithm

In this section, an example will be considered in order to illustrate how the algorithm, described in the previous section, works for finding a one-dimensional SQE-grid. That grid will be compared with the pertinent spectral quasi-equilibrium manifold, too. Let us consider the reaction (19). In this case, once a 3-component vector $\boldsymbol{m}$ has been chosen, the QEM equation can be found by solving the variational problem (27):

$$\begin{cases} G \to \min \\ (\boldsymbol{m}, \boldsymbol{c}) = \xi, \\ \boldsymbol{D}\boldsymbol{c} = 1. \end{cases} \tag{43}$$

In the sequel, the spectral quasi-equilibrium manifold [9,10] will be constructed. The Jacobian matrix $\boldsymbol{L}$ in the equilibrium point and its slowest left eigenvector $\boldsymbol{x}^s_l$ are:

$$\boldsymbol{L}(\boldsymbol{c}^{eq}) = \begin{bmatrix} -30 & -4.8 & 13.5 \\ -24 & -6.2 & 13.75 \\ 54 & 11 & -27.25 \end{bmatrix}, \quad \boldsymbol{x}^s_l = [\,0.8807, \quad -0.3905, \quad 0.2681\,]. \tag{44}$$

Solution to the problem (43), with the choice $\boldsymbol{m} = \boldsymbol{x}^s_l$, delivers the 1D SQEM for the case shown in Fig 1a. Let us rewrite (43) in a more explicit form:

$$\begin{cases} c_{0A} = 0.3072 + 0.7867\xi - 0.5180\phi(\xi), \\ c_{0B} = 0.6928 - 0.7867\xi - 0.4820\phi(\xi), \\ c_{0C} = \phi(\xi), \\ \frac{\partial G(\phi,\xi)}{\partial \phi} = 0, \quad \frac{\partial^2 G(\phi,\xi)}{\partial \phi^2} > 0, \end{cases} \tag{45}$$

where $\boldsymbol{c}_0 = [c_{0A}, c_{0B}, c_{0C}]$ is the solution of the problem (43), while ϕ denotes the relation between c_C and the reduced variable ξ on the SQEM. By using the G function (7), the problem (45) is equivalent to the equation

$$\left(\frac{0.3072 + 0.7867\xi - 0.5180\phi}{0.1}\right)^{-0.5180}\left(\frac{0.6928 - 0.7867\xi - 0.4820\phi}{0.5}\right)^{-0.4820}\left(\frac{\phi}{0.4}\right) - 1 = 0. \tag{46}$$

The solution of (46), by means of relations (45), gives the SQEM shown in Fig. 6a. We may now apply the QEG-algorithm described above, in order to make a comparison with the analytic solution just found. An orthonormal basis $\{\boldsymbol{\rho}_i\}$ in the null space of the matrix $\boldsymbol{D} = [\,1 \quad 1 \quad 1\,]$ has dimension $z = 2$ and can be chosen as follows:

$$\begin{cases} \boldsymbol{\rho}_1 = [-0.5774,\ 0.7887,\ -0.2113], \\ \boldsymbol{\rho}_2 = [-0.5774,\ -0.2113,\ 0.7887]. \end{cases} \tag{47}$$

Since the matrix $\boldsymbol{E}$ has the form:

$$\boldsymbol{E} = \begin{bmatrix} 0.8807 & -0.3905 & 0.2680 \\ 1 & 1 & 1 \end{bmatrix}, \tag{48}$$

a vector $\boldsymbol{t}$ spanning $\ker(\boldsymbol{E})$ is

$$\boldsymbol{t} = [-0.4229,\ -0.3934,\ 0.8163].$$

The system (38), in this example, simply reads:

$$\begin{cases} \langle \boldsymbol{t}, \boldsymbol{\rho}_1 \rangle \mu_1 + \langle \boldsymbol{t}, \boldsymbol{\rho}_2 \rangle \mu_2 = -(\boldsymbol{t}, \nabla G), \\ \mu_1^2 + \mu_2^2 = \varepsilon^2. \end{cases} \tag{49}$$

By solving (49) in a QEG-node $\boldsymbol{c}_n$, the shift vector $\hat{\delta}\boldsymbol{c}_n = \mu_1\boldsymbol{\rho}_1 + \mu_2\boldsymbol{\rho}_2$ allows to evaluate the new QEG-node $\boldsymbol{c}_{n+1} = \boldsymbol{c}_n + \hat{\delta}\boldsymbol{c}_n$. The QEG procedure, starting from the equilibrium point $\boldsymbol{c}^{\mathrm{eq}} = \boldsymbol{c}_0$, was performed twice, keeping uniform parameter $\varepsilon^2 = 10^{-3}$. The first time, by choosing the solution in such a way that $c_{B_{n+1}} < c_{B_n}$, the left branch of the SQE-grid was obtained; then, by imposing $c_{B_{n+1}} > c_{B_n}$, also the right branch was computed. The algorithm was terminated as soon as at least one component of the new node $\boldsymbol{c}_{n+1}$ becomes negative. The result, shown in Fig. 6b, proves that the SQE-grid is in excellent agreement with the analytical curve (SQEM).

Remark. Notice an "a priori" assumption that the SQEG can be uniquely parameterized by the variable c_B. Indeed, the choice between the two possible solutions of the problem (49) is done by checking the positivity of $\Delta c_B = c_{B_{n+1}} - c_{B_n}$. Such an approach might not work if the chosen parameter is not suitable for that purpose. For example, in the case of Fig. 6b, the variable c_C cannot be used because of a turning point. The latter aspect will be discussed in Section 8.

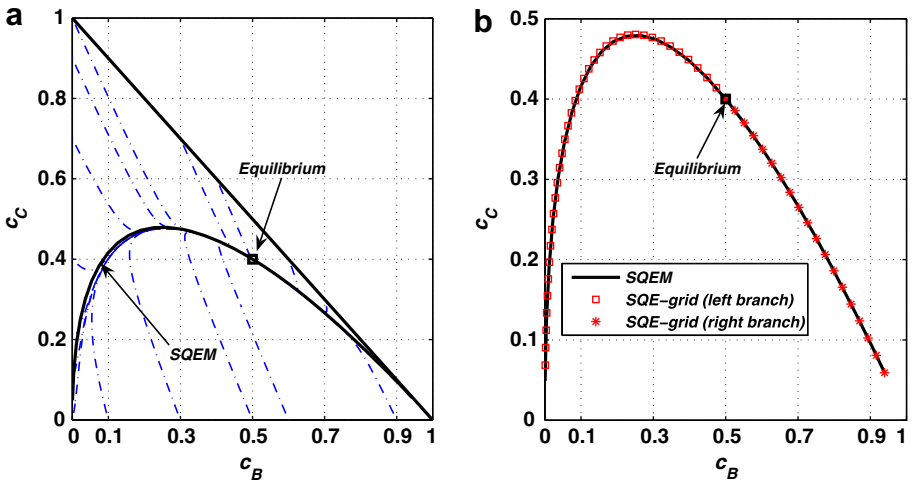

Fig. 6. (a) The bold curve is the SQE-manifold which was analytically evaluated by solving the (46). In that case the SQEM represents a very good approximation of the invariant manifold. (b) The SQE-manifold is compared to the SQE-grid, $\varepsilon^2 = 10^{-3}$.

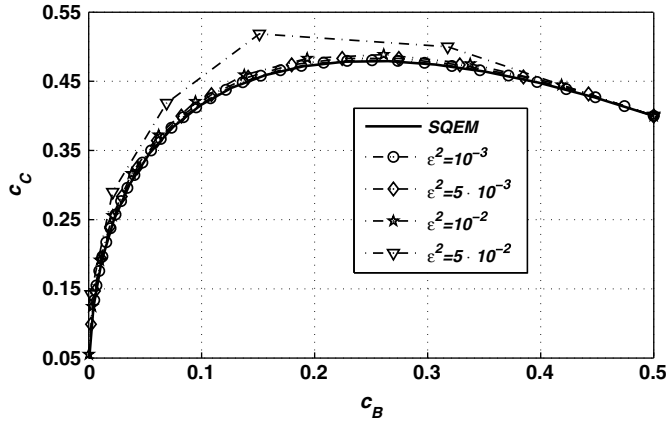

Fig. 7. SQEG Left branch of the case in Fig. 6b. Different approximations compared to the analytical solution (SQEM). Each grid is calculated by using a different parameter ε.

6.1. Grid spacing choice

There is no need to stress the importance of the grid spacing parameter ε for the QEG accuracy. In the case of Section 6, the SQEG was computed several times with different values of ε. The QEG algorithm is based on the linear approximation (34). Therefore, the smaller is $\|\hat{\delta}\boldsymbol{c}_n\| = \varepsilon$ the more accurate is the QEM description by means of the QEG. Nevertheless, the smaller is ε the larger is the number of times that the system (37) must be solved to have a grid of a fixed size. For this reason, we need to keep ε as large as possible. We estimated (at least the order of magnitude) the upper limit of spacing (ε_u) which gives a QEG "not far" from the relative QEM. From our numerical experiments, a reasonable value for that was $\varepsilon_u \cong 10^{-1}$. As Fig. 7 shows, the QEG is not far from the QEM even for a quite coarse grid ($\varepsilon > \varepsilon_u$).

7. Generalization to multi-dimensional grids

The QEG algorithm, which has been developed for constructing one-dimensional grids, can be modified in order to get multi-dimensional grids, whenever needed. From all reasonable extension strategies, two of them will be analyzed here: a *straightforward extension* and a *flag extension* (the flag extension, for invariant grids, was introduced in Ref. [11]). In the first case, the algorithm of Section 5 and the equation system (38) are tuned for a q-dimensional grid calculation. Here, the implicit assumption is that the grid dimension q is fixed and uniform everywhere in the phase space (like for the QEM construction itself). However, the second and more flexible approach, suitable for SQEG construction, was developed, too. In that case, the grid dimension can be varied at will.

7.1. The straightforward extension

According to the straightforward extension, if a node $\boldsymbol{c}_n$ close to the q-dimensional QEM is known, then a new node $\boldsymbol{c}_{n+1}$ can be added to the QE-grid by shifting $\boldsymbol{c}_n$:

$$\boldsymbol{c}_{n+1} = \boldsymbol{c}_n + \hat{\delta}\boldsymbol{c}_n, \quad \hat{\delta}\boldsymbol{c}_n = \sum_{i=1}^{z} \mu_i \boldsymbol{\rho}_i, \tag{50}$$

where $\{\boldsymbol{\rho}_i\}$ is a basis in the null space of matrix $\boldsymbol{D}$. The linear constraints of the problem (27) define the tangent space T to the G level surfaces in the new node $\boldsymbol{c}_{n+1}$. Let $\boldsymbol{c}$ be a generic point of T, the line l passing from $\boldsymbol{c}_{n+1}$ and $\boldsymbol{c}$ has the parametric form: $\boldsymbol{c} = \varphi\tilde{\boldsymbol{t}} + \boldsymbol{c}_{n+1}$, where $\tilde{\boldsymbol{t}}$ is the vector of T which spans l and φ is the parameter. The generalized form of the relations (30) is

$$\begin{cases} (\boldsymbol{m}_1, \boldsymbol{c}) = \varphi(\boldsymbol{m}_1, \tilde{\boldsymbol{t}}) + (\boldsymbol{m}_1, \boldsymbol{c}^i_{n+1}) \Rightarrow (\boldsymbol{m}_1, \tilde{\boldsymbol{t}}) = 0 \quad \forall \tilde{\boldsymbol{t}} \in T, \\ \vdots \\ (\boldsymbol{m}_q, \boldsymbol{c}) = \varphi(\boldsymbol{m}_q, \tilde{\boldsymbol{t}}) + (\boldsymbol{m}_q, \boldsymbol{c}^i_{n+1}) \Rightarrow (\boldsymbol{m}_q, \tilde{\boldsymbol{t}}) = 0 \quad \forall \tilde{\boldsymbol{t}} \in T, \\ (\boldsymbol{d}_i, \boldsymbol{c}) = \varphi(\boldsymbol{d}_i, \tilde{\boldsymbol{t}}) + (\boldsymbol{d}_i, \boldsymbol{c}^i_{n+1}) \Rightarrow (\boldsymbol{d}_i, \tilde{\boldsymbol{t}}) = 0 \quad \forall \tilde{\boldsymbol{t}} \in T, \end{cases} \tag{51}$$

which means that vector $\tilde{\boldsymbol{t}}$ belongs to the null space of the matrix $\boldsymbol{E}$ ($\ker \boldsymbol{E}$):

$$\boldsymbol{E} = \begin{bmatrix} \boldsymbol{m}_1 \\ \vdots \\ \boldsymbol{m}_q \\ \boldsymbol{D} \end{bmatrix}. \tag{52}$$

Now, the dimension of the basis $\{\boldsymbol{t}_j\}$ in $\ker(\boldsymbol{E})$ is $z - q$. Since the quasi-equilibrium condition requires that, among all the points $\boldsymbol{c}$ of T, $\boldsymbol{c}_{n+1}$ has the minimal value of G, the following orthogonality conditions hold:

$$(\nabla G(\boldsymbol{c}_{n+1}), \boldsymbol{t}_j) = 0 \quad \forall j = 1, \ldots, z - q. \tag{53}$$

For small vector $\hat{\delta}\boldsymbol{c}_n$, the approximation (34) can be used, so that the (53) become:

$$\sum_{i=1}^{z} \langle \boldsymbol{t}_j, \boldsymbol{\rho}_i \rangle \mu_i = -(\boldsymbol{t}_j, \nabla G(\boldsymbol{c}_n)) \quad \forall j = 1, \ldots, z - q. \tag{54}$$

As the system (54) shows, the larger is the QEM dimension (q) the smaller is the set of "mere" quasi-equilibrium equations available, while the number of unknowns remains constant (z). The closure of the rectangular system (54) requires q more equations and has only to do with the geometric structure which we want to provide the grid with (e.g. grid spacing, shift vector orientation in the phase space, etc). In general, the geometric structure of the grid under construction can be chosen at will: therefore there is no unique geometric closure for that system. However, one possible condition could be imposed, like in (37), by fixing the Euclidean norm of shift vector: $\|\hat{\delta}\boldsymbol{c}_n\| = \varepsilon$. Nevertheless, $(q - 1)$ geometric constraints are still missing. In order to illustrate how the geometric closure issue can be overcome, the case $q = 2$ will be considered in the sequel. For that case, a possible closure, which can be easily generalized, will be presented. If a two-dimensional QEG has to be constructed, then only one extra equation is needed to close the system:

$$\begin{cases} \sum_{i=1}^{z} \langle \boldsymbol{t}_j, \boldsymbol{\rho}_i \rangle \mu_i = -(\boldsymbol{t}_j, \nabla G(\boldsymbol{c}_n)) \quad \forall j = 1, \ldots, z - 2 \\ \|\hat{\delta}\boldsymbol{c}_n\| = \varepsilon. \end{cases} \tag{55}$$

Fig. 8 shows that all the possible solutions of (55) are located, as a "crown", near the QEM. A way to choose only two of them can be achieved by introducing a new fixed vector $\tilde{\boldsymbol{m}}$ and imposing a given angle ϑ between $\tilde{\boldsymbol{m}}$ and $\hat{\delta}\boldsymbol{c}_n$:

$$\sum_{i=1}^{z} (\tilde{\boldsymbol{m}}, \boldsymbol{\rho}_i) \mu_i = \|\hat{\delta}\boldsymbol{c}_n\| \cdot \|\tilde{\boldsymbol{m}}\| \cos\vartheta. \tag{56}$$

The choice $\vartheta = \pi/2$ proves to be particularly convenient, as (56) becomes:

$$\sum_{i=1}^{z} (\tilde{\boldsymbol{m}}, \boldsymbol{\rho}_i) \mu_i = 0. \tag{57}$$

Eq. (57) allows to write a closed system:

$$\begin{cases} \sum_{i=1}^{z} \langle \boldsymbol{t}_j, \boldsymbol{\rho}_i \rangle \mu_i = -(\boldsymbol{t}_j, \nabla G(\boldsymbol{c}_n)) \quad \forall j = 1, \ldots, z - 2, \\ \sum_{i=1}^{z} (\tilde{\boldsymbol{m}}, \boldsymbol{\rho}_i) \mu_i = 0, \\ \|\hat{\delta}\boldsymbol{c}_n\| = \varepsilon, \end{cases} \tag{58}$$

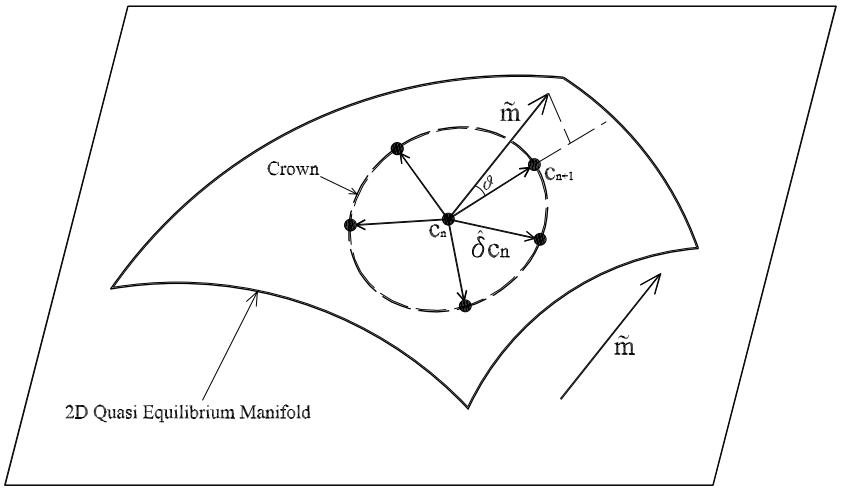

Fig. 8. 2D quasi-equilibrium manifold. Location of solutions of the system (55) in the phase space.

where the extra information, through ε and $\tilde{\boldsymbol{m}}$, concerns the grid spacing and the phase space zone of interest where the grid is constructed. In general, the geometric closure of (54) can be achieved when $(q-1)$ independent vectors $\{\tilde{\boldsymbol{m}}_i\}$ and the parameter ε are fixed. Here, we present an approach which allows to get a rectangular structured grid. The general form of (58) is

$$\begin{cases} \sum_{i=1}^{z} \langle \boldsymbol{t}_j, \boldsymbol{\rho}_i \rangle \mu_i = -(\boldsymbol{t}_j, \nabla G(\boldsymbol{c}_n)) & \forall j = 1, \ldots, z-q, \\ \sum_{i=1}^{z} (\tilde{\boldsymbol{m}}_j, \boldsymbol{\rho}_i) \mu_i = 0 & \forall j = 1, \ldots, q-1, \\ \|\hat{\delta}\boldsymbol{c}_n\| = \varepsilon. \end{cases} \tag{59}$$

The q-dimensional grid construction is split in q subsequent steps. Starting from the equilibrium $\boldsymbol{c}^{\mathrm{eq}}$, system (59) is solved by choosing $(q-1)$ $\boldsymbol{m}_j$ vectors among the q available and imposing: $\tilde{\boldsymbol{m}}_j = \boldsymbol{m}_j \ \forall j = 1, \ldots, q-1$. In this way, a first set of QEG nodes is attained as soon as ε is known. Now, starting from each of these points, the system (59), by using a different combination of $\boldsymbol{m}_j$ vectors, gives some more nodes. The procedure ends (qth step) when all the possible different combinations of $(q-1)$ vectors $\{\boldsymbol{m}_j\}$ are exhausted. In Section 9, this method will be explained by means of an illustrative example.

7.2. The flag extension

A multi-dimensional QE-grid construction becomes non-trivial especially when q becomes large. As reported in Section 7.1, the straightforward extension requires the introduction of some additional vectors $\tilde{\boldsymbol{m}}_j$. The flag extension can be applied when a SQEG is searched. That procedure is based on the algorithm presented in Section 5 and it naturally leads to a rectangular structured grid. The idea behind is simple and makes this method flexible and suitable for constructing high-dimensional rectangular grids. Let us assume that q is the grid dimension and the q SQE-vectors $\{\boldsymbol{m}_1, \ldots, \boldsymbol{m}_q\}$ are fixed. Let $\boldsymbol{m}_1$ be the slowest eigenvector (corresponding to the smallest eigenvalue by absolute value), $\boldsymbol{m}_2$ the second slowest and so forth. The grid construction is achieved in q subsequent steps. In each step one more dimension is added to the grid. At the beginning, by using $\boldsymbol{m} = \boldsymbol{m}_1$, the algorithm in Section 5 provides the 1D quasi-equilibrium grid. Now, starting from any node $\boldsymbol{c}^*$ of the latter grid, a new 1D QEG is constructed where $\boldsymbol{m} = \boldsymbol{m}_2$. In this case, the second QEG represents a trajectory on the 2D-manifold attracted to the slowest 1D-manifold in the node $\boldsymbol{c}^*$, once the fast dynamics is exhausted (see Fig. 9). G depends on the equilibrium point $\boldsymbol{c}^{\mathrm{eq}}$: $G = G(\boldsymbol{c}, \boldsymbol{c}^{\mathrm{eq}})$. Since $\boldsymbol{c}^*$ can be considered as a "local equilibrium" for the fast motion, the second 1D grid is obtained by minimizing $G = G(\boldsymbol{c}, \boldsymbol{c}^*)$. Once the previous step is completed, the grid can be extended in the third dimension by

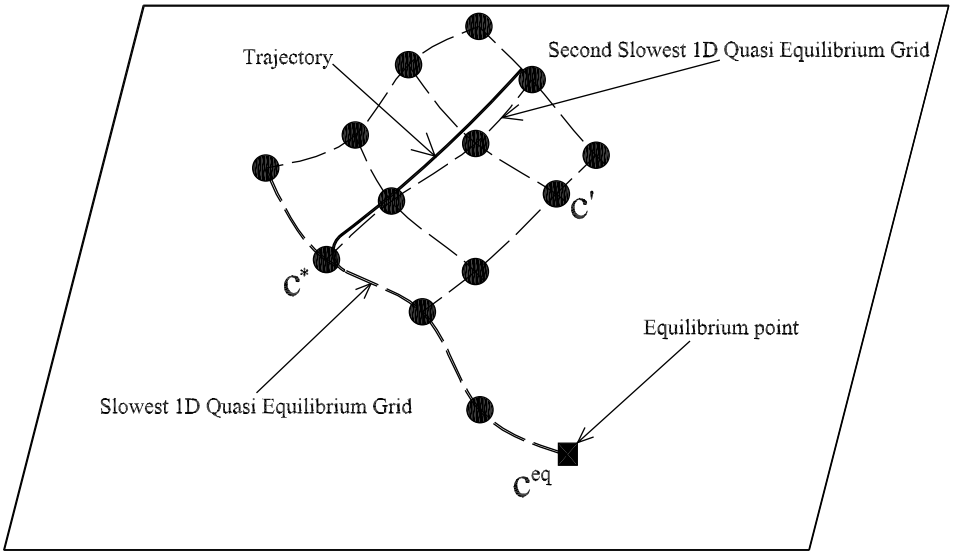

Fig. 9. A 2D flag. Once the 1D quasi-equilibrium grid is found, from each node $\boldsymbol{c}^*$, new 1D quasi-equilibrium grids are added. The second slowest 1D grid represents the solution trajectory collected by the first 1D quasi-equilibrium grid in the node $\boldsymbol{c}^*$.

adding, in each node $\boldsymbol{c}'$ of the new 2D grid, a 1D QEG where $\boldsymbol{m} = \boldsymbol{m}_3$ and $G = G(\boldsymbol{c}, \boldsymbol{c}')$. In this way, the procedure is performed up to a q-dimensional grid. By extending partially the previous grid, it is possible to construct grids whose dimension is different in different phase space zones. It is worth mentioning that the straightforward and the flag extension deliver two different objects: the first one just gives the quasi-equilibrium grid "brute force", while the second one is its convenient "approximation" which has some useful features as it will be illustrated in the sequel. First of all, the flag grid does not demand any extra vector for the geometric closure and the grid dimension can be easily varied in different phase space zones. Secondly, if a grid refinement procedure (MIG) is used in order to get an invariant grid, as a refinement of the quasi-equilibrium one [10], then the flag extension becomes a useful tool. Indeed, let us assume that a multi-dimensional invariant grid is required in order to reduce a given model. A possible strategy might be given by a "hybrid procedure" where the QEG algorithm and the MIG method are alternatively used according to the sequence:

- 1D quasi-equilibrium grid construction (slowest grid);
- MIG refinements until the 1D invariant grid is obtained;
- flag extension from 1D invariant grid to 2D quasi-equilibrium grid;
- MIG refinements until the 2D invariant grid is obtained;
- flag extension from 2D invariant grid to 3D quasi-equilibrium grid;
- MIG refinements...

7.3. Beyond SQEG: GQEG and SEGQEG

The latter suggestion sheds light on one more option which, if implemented during the flag extension, allows to go beyond the SQEG approximation of the slow invariant manifold. Let us assume that the hybrid procedure of Section 7.2 is employed and a k-dimensional invariant grid (let $\boldsymbol{c}^*$ be its generic node) has to be extended to a $(k+1)$-dimensional grid. This grid approximates the $(k+1)$-dimensional invariant grid better than the SQEG does, if in each invariant grid node $\boldsymbol{c}^*$ the vector $\boldsymbol{m}$ is chosen as the $(k+1)$th slowest left eigenvector of the Jacobi matrix $\boldsymbol{L}(\boldsymbol{c}^*)$. According to [9], here a considerable simplification can be achieved by replacing the full Jacobian $\boldsymbol{L}(\boldsymbol{c}^*)$ with:

$$\boldsymbol{L}^{\mathrm{sym}}(\boldsymbol{c}^*) = \frac{1}{2}(\boldsymbol{L}(\boldsymbol{c}^*) + \boldsymbol{H}^{-1}\boldsymbol{L}^{\mathrm{T}}(\boldsymbol{c}^*)\boldsymbol{H}), \tag{60}$$

where $\boldsymbol{L}^{\mathrm{T}}$ is the ordinary transposition, and $\boldsymbol{H}$ is evaluated at the point $\boldsymbol{c}^*$, too. Matrix $\boldsymbol{L}^{\mathrm{sym}}$ is symmetric with respect to the entropic scalar product (8). For that reason the spectral decomposition will be much more viable (see also Ref. [10]). Those two new approximations will be named: *guided quasi-equilibrium grid* (GQEG) when the full Jacobian $\boldsymbol{L}(\boldsymbol{c}^*)$ is used, while *symmetric entropic guided quasi-equilibrium grid* (SEGQEG) if $\boldsymbol{L}^{\mathrm{sym}}$ replaces the full matrix. In order to give an idea about the effort needed, for example in a SEGQEG construction, let us consider a two-dimensional grid. In that case, the spectral decomposition of a symmetric operator is performed only over the nodes of a one-dimensional grid. Moreover, also a criterion, for getting a multi-dimensional grid, naturally applies: if at the node $\boldsymbol{c}^*$ of the k-dimensional invariant grid, the ratio $|\lambda_{k+1}|/|\lambda_k|$ (between eigenvalues of $\boldsymbol{L}$ or $\boldsymbol{L}^{\mathrm{sym}}$, respectively) is not larger than a fixed threshold, the $(k+1)$-dimensional grid will not be extended at that point. In this way, the grid dimension q is generally not uniform in the phase space. Several techniques suggested above are only some reasonable ones. The flexibility of the method proposed allows to set up different procedures, still based on the quasi-equilibrium grid approach: the QEG system (54) supplied with a geometrical closure.

8. Grid construction

The construction of a QEG is entirely local. Without loss of generality, we can refer to the algebraic system (37). It only depends on the local gradient $\nabla G(\boldsymbol{c}_n)$ and second derivative matrix $\boldsymbol{H}(\boldsymbol{c}_n)$. For that reason, in order to compute the unknown vector $\hat{\delta}\boldsymbol{c}_n$, no "a priori" grid parameterization is requested. However, a criterion able to choose between the two solutions of (37), without getting into troubles in the case of turning points, is needed. We may overcome that problem with the help of a proper parameterization, as suggested in Section 6. In general, a QEG has a natural parameterization which is simply given by the variables ξ_i in (27). Let us refer to the one-dimensional construction described in Section 5. Here, starting from the equilibrium point $\boldsymbol{c}^{\mathrm{eq}}$ as first node of the grid, the subsequent points can be chosen by imposing the positivity of the inner product $(\boldsymbol{m}, \hat{\delta}\boldsymbol{c})$. In general, by extending the grid outwards from a zone of phase space close to the steady point, one reaches regions where the solution becomes unphysical (such as negative concentrations of some species). In that case, the evaluated node is cut off while the procedure starts again from $\boldsymbol{c}^{\mathrm{eq}}$. Now, solutions $\hat{\delta}\boldsymbol{c}_n$ with $(\boldsymbol{m}, \hat{\delta}\boldsymbol{c}) < 0$ are considered till non-negative concentrations are found. Let n be the dimension of the phase space. The one-dimensional grid is described as an ordered sequence of nodes. Those nodes can be collected in n one-dimensional arrays, where in each of them a different specie is stored. However, different criteria for choosing the solutions, not based on the grid parametrization, may be also used. Let $\boldsymbol{c}_0 = \boldsymbol{c}^{\mathrm{eq}}$. Let $\boldsymbol{c}_1^{\mathrm{I}}$ and $\boldsymbol{c}_1^{\mathrm{II}}$ be the two solutions to (38) at $\boldsymbol{c}_0$. Assume that the second grid node is $\boldsymbol{c}_2 = \boldsymbol{c}_1^{\mathrm{I}}$. The third grid node can be chosen such that the Euclidean distance $\|\boldsymbol{c}_3 - \boldsymbol{c}_0\|$ is maximum. Indeed, one of the two solutions evaluated at $\boldsymbol{c}_2$ is located close to $\boldsymbol{c}_0$: they would overlap if the quasi-equilibrium grid nodes were exactly on the pertinent quasi-equilibrium manifold. In this way, at any grid point $\boldsymbol{c}_n$, by choosing the solution which has the maximum distance $\|\boldsymbol{c}_{n+1} - \boldsymbol{c}_{n-1}\|$, the first branch of the grid is computed. Once the boundary is reached, the procedure is terminated. By means of the same criterion, the second grid branch is constructed starting from $\boldsymbol{c}_0$ and choosing the subsequent node as $\boldsymbol{c}_2 = \boldsymbol{c}_1^{\mathrm{II}}$. This strategy can be applied also for multi-dimensional grids, if the flag extension is used. Indeed, once the one-dimensional grid is found, the procedure can be applied as previously described. Now the starting point is any node of that grid. In this way, a two-dimensional grid is built up. Here the nodes are stored in n two-dimensional arrays where the previous arrays are embedded as a single column. Similarly, the latter grid can be extended in the third dimension and so on.

9. 2D grid example: hydrogen oxidation reaction

Let us consider a model for hydrogen oxidation reaction where six species H_2 (hydrogen), O_2 (oxygen), H_2O (water), H, O, OH (radicals) are involved in six steps in a closed system under constant volume and temperature (from Ref. [12], p. 291):

$$\begin{cases} 1.\,H_2 \leftrightarrow 2H, & k_1^+ = 2, \\ 2.\,O_2 \leftrightarrow 2O, & k_2^+ = 1, \\ 3.\,H_2O \leftrightarrow H + OH, & k_3^+ = 1, \\ 4.\,H_2 + O \leftrightarrow H + OH, & k_4^+ = 10^3, \\ 5.\,O_2 + H \leftrightarrow O + OH, & k_5^+ = 10^3, \\ 6.\,H_2 + O \leftrightarrow H_2O, & k_6^+ = 10^2. \end{cases} \tag{61}$$

The conservation laws are:

$$\begin{cases} 2c_{H_2} + 2c_{H_2O} + c_H + c_{OH} = b_H = 2, \\ 2c_{O_2} + c_{H_2O} + c_O + c_{OH} = b_O = 1, \end{cases} \tag{62}$$

when the equilibrium point is fixed, for example

$$c_{H_2}^{eq} = 0.27, \quad c_{O_2}^{eq} = 0.135, \quad c_{H_2O}^{eq} = 0.7, \quad c_H^{eq} = 0.05, \quad c_O^{eq} = 0.02, \quad c_{OH}^{eq} = 0.01, \tag{63}$$

then the rest of the rate constants k_i^- are calculated using the detailed balance principle (4). The system under consideration is fictitious in the sense that the subset of equations corresponds to the simplified picture of this chemical process and the rate constants reflect only orders of magnitude for relevant real-word systems. We assume that the Lyapunov function G has the ideal gas form:

$$G = \sum_{i=1}^{6} c_i \left[\ln\left(\frac{c_i}{c_i^{eq}}\right) - 1 \right]. \tag{64}$$

Here, we are interested in the 2D SQEG construction. Two left eigenvectors of Jacobian matrix $\boldsymbol{L}(\boldsymbol{c}^{eq})$ are:

$$\begin{cases} \boldsymbol{x}_l^{s1} = [-0.577,\ -0.568,\ 0.225,\ 0.0482,\ 0.0666,\ -0.536], \\ \boldsymbol{x}_l^{s2} = [0.00682,\ -0.00595,\ 0.0221,\ -0.7,\ -0.713,\ 0.423], \end{cases} \tag{65}$$

where $\boldsymbol{x}_l^{s1}$ and $\boldsymbol{x}_l^{s2}$ are the slowest and the second slowest one, respectively.

9.1. The 2D straightforward extension

In order to get a 2D SQEG for that example, the straightforward extension was used as first strategy. Matrices $\boldsymbol{D}$ and $\boldsymbol{E}$ take now the form:

$$\boldsymbol{D} = \begin{bmatrix} 2 & 0 & 2 & 1 & 0 & 1 \\ 0 & 2 & 1 & 0 & 1 & 1 \end{bmatrix}, \quad \boldsymbol{E} = \begin{bmatrix} -0.577 & -0.568 & 0.225 & 0.0482 & -0.0666 & -0.536 \\ 0.00682 & -0.00595 & 0.0221 & -0.7 & -0.713 & 0.423 \\ 2 & 0 & 2 & 1 & 0 & 1 \\ 0 & 2 & 1 & 0 & 1 & 1 \end{bmatrix}. \tag{66}$$

As suggested in the end of Section 7.1, the procedure has been started from the equilibrium point and it was split in two subsequent steps. At the beginning, the system (58) was solved by imposing $\varepsilon^2 = 0.5 \times 10^{-3}$ and $\tilde{\boldsymbol{m}} = \boldsymbol{x}_l^{s2}$: in this way, the grid nodes, denoted by circles, in Fig. 10 were obtained. During the second step, (58) was solved by starting from any circle: this time, the geometric constraints were $\varepsilon^2 = 0.5 \times 10^{-3}$ and $\tilde{\boldsymbol{m}} = \boldsymbol{x}_l^{s1}$. During that step, in each circle, the horizontal dots of Fig. 10 were found, too.

9.2. The 2D flag extension

Here we apply the flag extension procedure. For that the 1D spectral quasi-equilibrium grid is needed. Matrices $\boldsymbol{D}$ and $\boldsymbol{E}$ are in this case:

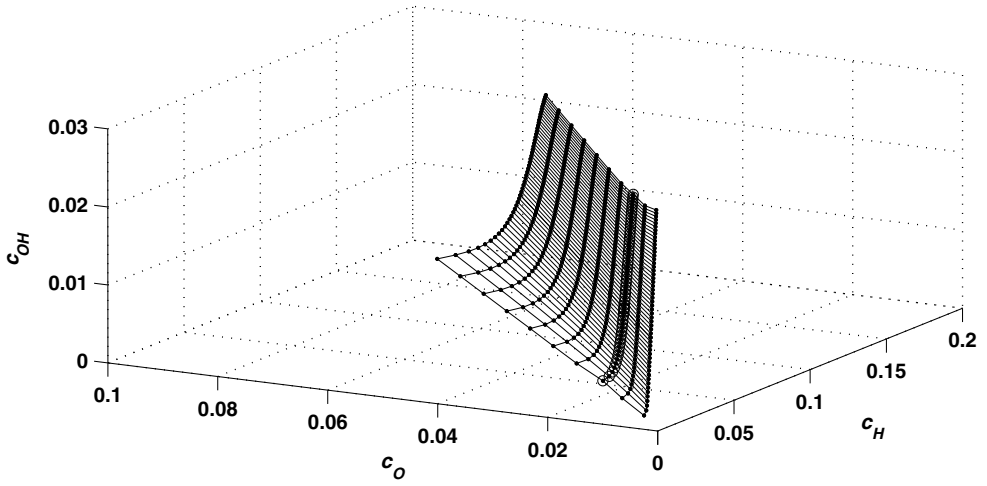

Fig. 10. The 2D SQEG constructed by using the straightforward extension with $\varepsilon^2 = 0.5 \times 10^{-3}$: projection into the phase-subspace $(c_{\mathrm{H}}, c_{\mathrm{O}}, c_{\mathrm{OH}})$.

$$\boldsymbol{D} = \begin{bmatrix} 2 & 0 & 2 & 1 & 0 & 1 \\ 0 & 2 & 1 & 0 & 1 & 1 \end{bmatrix}, \quad \boldsymbol{E} = \begin{bmatrix} -0.577 & -0.568 & 0.225 & 0.0482 & 0.0666 & -0.536 \\ 2 & 0 & 2 & 1 & 0 & 1 \\ 0 & 2 & 1 & 0 & 1 & 1 \end{bmatrix}. \tag{67}$$

Starting from the equilibrium point $\boldsymbol{c}^{\mathrm{eq}}$, the system (38) was solved by fixing $\varepsilon^2 = 1 \times 10^{-3}$ (see Fig. 11). The flag extension was used to get a 2D grid out of the 1D one. Now, the new matrix $\boldsymbol{E}$ reads:

$$\boldsymbol{E} = \begin{bmatrix} 0.00682 & -0.00595 & 0.0221 & -0.7 & -0.713 & 0.423 \\ 2 & 0 & 2 & 1 & 0 & 1 \\ 0 & 2 & 1 & 0 & 1 & 1 \end{bmatrix},$$

while the Lyapunov function G has the form:

$$G = \sum_{i=1}^{6} c_i \left[\ln\left(\frac{c_i}{c_i^*}\right) - 1 \right], \tag{68}$$

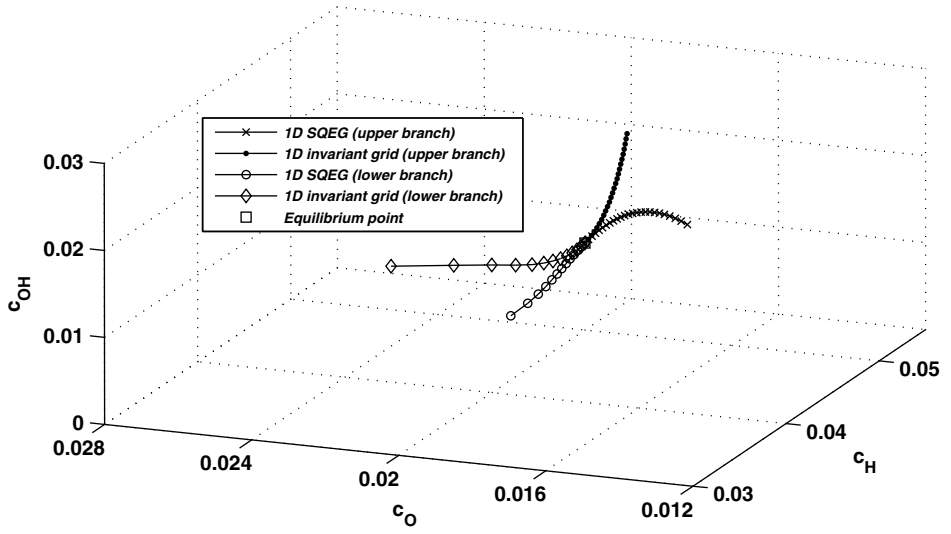

Fig. 11. 1D spectral quasi-equilibrium Grid with $\varepsilon^2 = 1 \times 10^{-3}$ compared to the 1D invariant grid obtained by MIG refinements.

where $\boldsymbol{c}^* = [c_1^*, \ldots, c_6^*]$ is any 1D grid node which is extended in the second dimension (see Fig. 9). Fig. 12a and b show two different 2D SQE-grids: the first one is obtained by extending the 1D SQE-grid, while in the second case the 1D invariant grid is used. In other words, the latter result was attained by the "hybrid procedure" QEGA + MIG suggested in the end of Section 7.2. For both cases, in the second dimension, the grid spacing was $\varepsilon^2 = 0.5 \times 10^{-3}$.

9.3. The 2D GQEG and SEGQEG

Finally, the GQEG and SEGQEG approximations are computed for the hydrogen oxidation reaction (61) (case 1 in Fig. 13). The grid spacing was kept uniform, $\varepsilon^2 = 0.45 \times 10^{-3}$. Each grid has 10×15 nodes and it is compared with both the SQEG (straightforward extension) of similar size (check Table 1) and the invariant grid. The invariant grid was obtained by refining the approximations through the MIG procedure. All those grids lie quite close to each other. However, a "more pathological" case 2 was also analyzed (see Fig. 14). Now, the SQEG, far from the equilibrium, presents a remarkable deviation from the invariant grid: now the rate constant set is taken as $k_1^+ = 20$, $k_2^+ = 1$, $k_3^+ = 1$, $k_4^+ = 10^3$, $k_5^+ = 10^3$, $k_6^+ = 10^2$, while the equilibrium point coordinates are still given by (63). For that case, the SQEG, GQEG and SEGQEG were constructed by choosing the grid spacing and size as for the previous case 1. Note that all the grids were partially extended only below the equilibrium point in the phase space zone where they present the largest deviation from the invariant grid. This time those three approximations have a low invariance defect only near the equilibrium. In order to estimate how far each grid is from the invariant one, the following procedure is implemented. A 10×15 matrix, collecting in any grid node an invariance defect measure, is constructed. As suggested in [10], that local measure may be $\sqrt{(\boldsymbol{\Delta}, \boldsymbol{\Delta})/(\boldsymbol{J}, \boldsymbol{J})}$, where $\boldsymbol{\Delta}$ and $\boldsymbol{J}$ are the invariance defect (12) and the vector field of (5), respectively. $\boldsymbol{\Delta}$ is evaluated by using the thermodynamic projector (17). By averaging over all the invariance defect measures, the mean invariance defect is provided: results for both cases are condensed in Table 1. Note that the adopted invariance defect measure is dimensionless as it compares the invariance defect with the vector field. Calculations prove that the GQEG is better than the SQEG (straightforwardly extended);

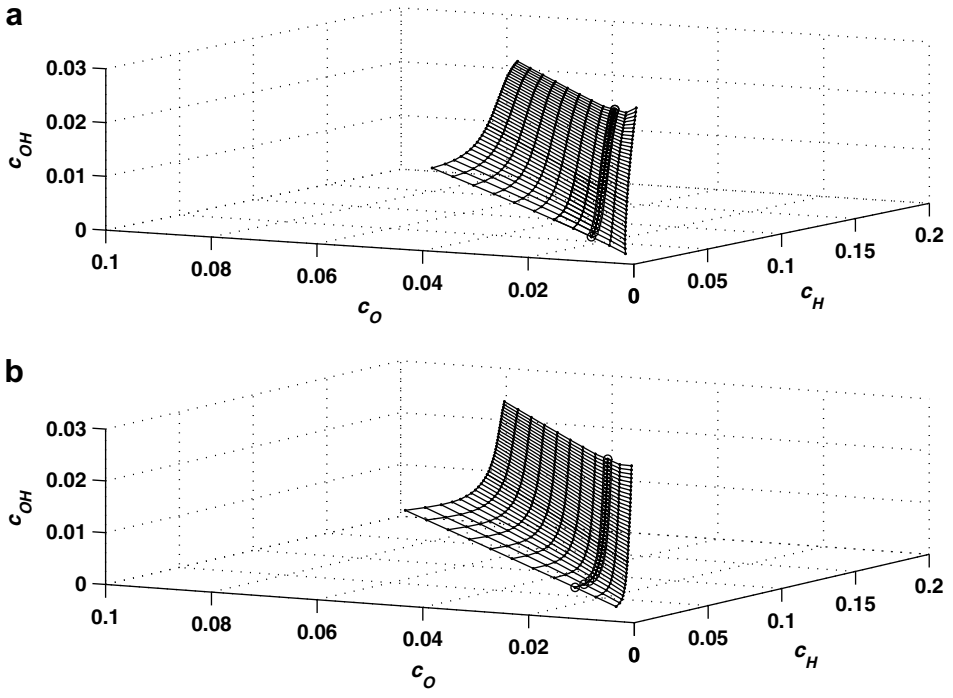

Fig. 12. The flag extension. (a) 2D SQEG (dots) extended from the 1D SQEG with $\varepsilon^2 = 1 \times 10^{-3}$ (circles). (b) 2D SQEG (dots) extended from the 1D invariant grid (circles). In the second dimension $\varepsilon^2 = 0.5 \times 10^{-3}$.

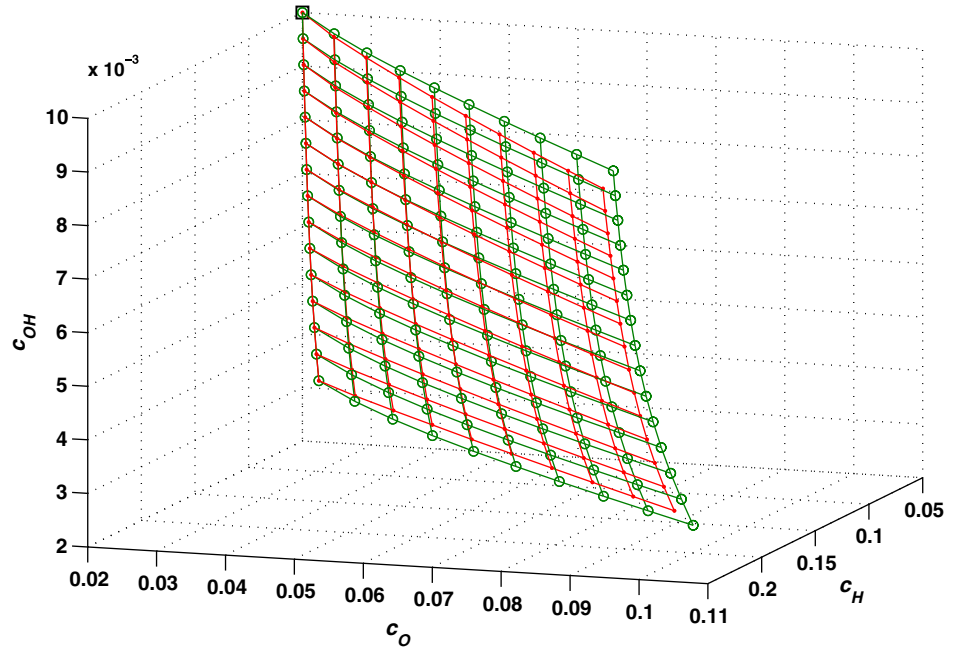

Fig. 13. Case 1: $k_1^+ = 2, k_2^+ = 1, k_3^+ = 1, k_4^+ = 10^3, k_5^+ = 10^3, k_6^+ = 10^2, \varepsilon^2 = 0.45 \times 10^3$. Two grids formed by 10×15 nodes. A 2D GQEG (dots) and a 2D invariant grid (circles) are reported. The grids are partially extended below the equilibrium point (square).

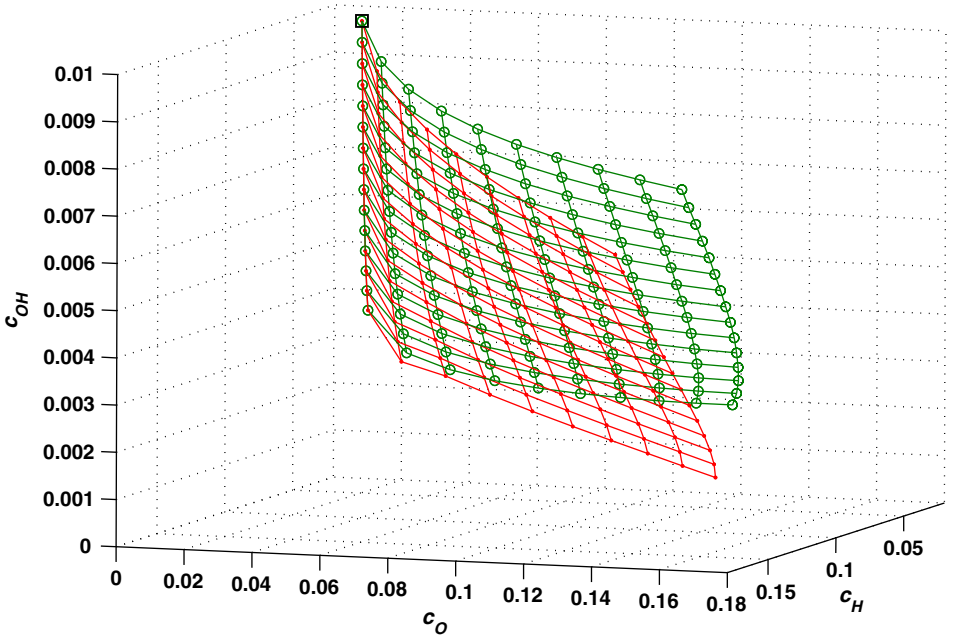

Fig. 14. Case 2: $k_1^+ = 20, k_2^+ = 1, k_3^+ = 1, k_4^+ = 10^3, k_5^+ = 10^3, k_6^+ = 10^2, \varepsilon^2 = 0.45 \times 10^3$. Two grids formed by 10×15 nodes. A 2D GQEG (dots) and a 2D invariant grid (circles) are reported. The grids are partially extended below the equilibrium point (square).

nevertheless the SEGQEG construction, since it requires a much lower computational effort and still has an error similar to the GQEG, is recommended when the SQEG is considered not satisfactory (e.g. large mean defect).

Table 1
Mean invariance defect (dimensionless): three approximations of the invariant grid under comparison for the hydrogen oxidation reaction

	1. Case	2. Case
SQEG	0.318	0.645
GQEG	0.238	0.460
SEGQEG	0.303	0.491

In case 1, the parameter set is: $k_1^+ = 2$, $k_2^+ = 1$, $k_3^+ = 1$, $k_4^+ = 10^3$, $k_5^+ = 10^3$, $k_6^+ = 10^2$, $\varepsilon^2 = 0.45 \times 10^3$. In case 2, the parameter set is: $k_1^+ = 20$, $k_2^+ = 1$, $k_3^+ = 1$, $k_4^+ = 10^3$, $k_5^+ = 10^3$, $k_6^+ = 10^2$, $\varepsilon^2 = 0.45 \times 10^3$.

10. Discussion of the method

The presented approach is implicitly based on a hypothesis about connected slow invariant manifold. This is not always the case. Further aspects of the applicability of quasi-equilibrium approximation can be found in Refs. [9–12,43]. Nevertheless, when that hypothesis is valid, the rationale behind the fact that quasi-equilibrium manifolds represent an approximation of the slow invariant manifold, in the case of fast and slow motion decomposition (i.e. gap in the eigenvalues of the Jacobi matrix) and existence of a Lyapunov function G, is illustrated in Fig. 15. For such systems, a solution trajectory that approaches the slow invariant manifold, during the initial fast transient, only moves (approximately) in the fast subspace L. Since G is decreasing in the course of the fast motions, points $\boldsymbol{c}^*$ which minimize G on the affine spaces $(\boldsymbol{c}^* + L)$ are expected to be located close to the slow invariant manifold. However, when the construction of the slow invariant manifold needs to be addressed, the subspace L is not known "a priori" and it generally depends on the point $\boldsymbol{c}^*$. Hence, for constructing the quasi-equilibrium approximation, a guess of L is needed. Here, it is important to discuss some connections with the work of other authors. It is very well known that for some closed reactive systems, the Lyapunov function is given by thermodynamic potentials (e.g. Gibbs free energy if temperature and pressure are constant, entropy if energy and density are constant, etc.). Notice that the very first use of entropy maximization has to be referred to the classical work of Gibbs [1] and later addressed to Jaynes [2], Kogan and Rozonoer [3,4]. More generally, the quasi-equilibrium approach constitutes an attempt in statistical mechanics to link microscopic models to the macroscopic ones providing the latter with a closure. For example, in [7,8], equations describing quasi-equilibrium dynamics for polymer are presented. Regarding the chemical kinetics, also the method of rate controlled constrained equilibrium (RCCE), introduced by Keck and Gillespie [19],

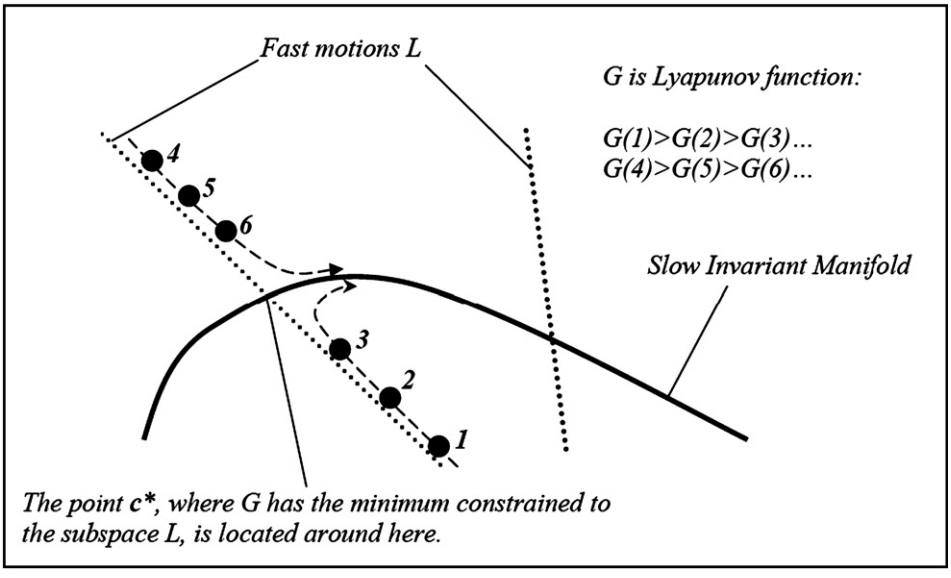

Fig. 15. Implication of fast-slow decomposition and existence of a Lyapunov function G.

reviewed by Keck (1990) and further developed in the recent literature [22,23], can be related to the quasi-equilibrium approximation. An interesting geometric viewpoint of RCCE is given by Tang and Pope [21]. After choosing a set of constraints, RCCE method makes use of the assumption that chemical systems evolve according to a sequence of quasi-equilibrium states which are function of the instantaneous values of such constraints. Those constraints are related to the unknown fast subspace L and need to be chosen. In general, some variable constraints (total moles, active valences, etc.), in addition to elemental fixed constraints (total number of atoms), are imposed for minimizing the thermodynamic potential and getting the species constrained composition. In order to evaluate that constrained-equilibrium point, the Lagrange multipliers problem can be iteratively solved via available routines (see e.g. STANJAN [24]). Nevertheless, some differences between the two approaches need to be stressed. The QEGA is not an iterative procedure. Assuming that the steady state (or any other point close to such a QE-manifold) is known, it aims at computing a set of nodes in the phase space (QEG) approximating the quasi-equilibrium manifold. Since the latter grid is generally not invariant [21] (see also Table 1), it has to be tabulated and used only as first approximation in the MIG procedure described in Sections 3.2.6 and 3.2.7. Moreover, the suggested construction uses a special choice of the constraints, based on spectral decomposition of Jacobian at few points, for constructing SQEG, GQEG and SEGQEG. As the above examples show, such approximate grids are accurate only in a neighborhood of equilibrium (see also [10]). However, here we are not interested in the quasi-equilibrium dynamics per se. For that reason, once a grid is constructed by the QEGA, it needs to be refined via MIG iterations. Only the fixed point of the MIG method (invariant grid) is considered for integrating the reduced system. The latter aspect of model reduction is going to be illustrated in a forthcoming publication. As stated elsewhere in the paper, the classical approach to the problem of minimization of convex functions subject to constraints is the Lagrange multipliers method. When the number of species becomes large enough, a non-linear system needs to be solved through Newton–Raphson iterations for each chemical constrained-equilibrium point. Alternatively, the chemical composition of ideal gas mixtures may be evaluated, through the more stable Gibbs function continuation method, by integrating a set of ODEs [20]. However, here we suggest a grid-based approach to that problem. Indeed, the quasi-equilibrium algorithm is a tool that aims at extending automatically a grid around a given point in the phase space. Although such a procedure is based on the geometry behind the Lagrange multipliers method, as explained in Sections 7.2 and 7.3 it may also deliver approximations of the slow invariant manifold even more accurate than a quasi-equilibrium grid itself (see Table 1). Indeed, a multi-dimensional GQEG (or SEGQEG) is not only based on the minimization of a thermodynamic potential, but it also takes into account information from the Jacobi matrix evaluated at few points. Therefore, a GQEG is not a "pure" quasi-equilibrium approximation any longer. In that case, the flag extension allows both the construction of objects of varying dimension and implementation of hybrid procedure: QEGA + MIG. On the other hand, in such a flexible grid-based approach, in order to compute an uniform grid the number of points scales as ε^{-q}. Where q is the grid dimension, while ε is the small grid parameter. In general, ε is not kept constant. For instance, during a hierarchical construction (flag extension), it is convenient to use a coarser grid for describing the lowest-dimensional manifolds. During our calculations, the criterion used to end the grid was based on non-negative concentrations. As soon as the evaluated grid point leaves the admissible phase space, it is cut and the procedure terminated (see also Section 8). That may seem inefficient, but it is worth to point out that the construction of the quasi-equilibrium grid is done only once and then tabulated for a later use in MIG procedure.

11. Conclusions

In this paper, the problem of quasi-equilibrium manifold approximation by means of a grid description is addressed. To this end, the notion of quasi-equilibrium grid (QEG) is introduced and a proper algorithm to construct it, in any dimension, is suggested (QEGA). It has been shown, through illustrative examples, that the QEGA gives a very good QEM approximation. The QEGA is a completely numerical procedure and it reveals particularly suitable for providing the MIG procedure with the first SIM approximation. As it has been illustrated, some proper hybrid procedures QEGA + MIG, where both methods are alternatively used, allow to obtain accurate SIM descriptions. In particular, it was proved that two special QEGA + MIG procedures deliver enhanced approximations of SIM: the *guided quasi-equilibrium grid* and the *symmetric entropic guided*

quasi-equilibrium grid. Here, we want to stress the two major advantages of the method proposed. First of all, it is a numerical algorithm which only deals with nodes sets in the concentration space. Moreover, it is a local construction: namely, the computation of a new node $\boldsymbol{c}_{n+1}$, which has to be added to the grid, only depends on the previous neighbor $\boldsymbol{c}_n$. Those two aspects make the QEG construction suitable for numerical applications and parallel realizations.

The suggested method was also applied to a realistic non-isothermal system reacting according to the detailed hydrogen mechanism described in [13]. The interested reader can find a detailed account in [14], where an estimation of the computational time for generating QE-grid nodes on a single processor is also given.

Finally, it is not excluded that the QEGA is applicable not only for model reduction, but in different fields, too. Indeed, it was mentioned that the QEM notion already is exploited for some applications in Lattice Boltzmann schemes simulations. More generally, the QEGA is a numerical tool which can be used to find a grid-based approximation for the locus of minima of a convex function under some linear constraints. In this paper we focused only on the geometry of the model reduction, that is, construction of slow invariant manifolds approximations. The implementation of grid-based integrators for dynamic equations will be presented in a separate publication.

Acknowledgments

Prof. A.N. Gorban is gratefully acknowledged for the fruitful discussions about the concept of quasi-equilibrium manifold and for suggesting the reaction mechanism (19). We thank Prof. K.B. Boulouchos and Dr. C.E. Frouzakis for discussions and suggestions. One of the authors (E.C.) is grateful to Prof. S.H. Lam and D.A. Goussis for the discussions during the Workshop on Model Reduction in Reacting Flow 2007. This work was partially supported by SNF (Project 200021-107885/1), by BFE (Project 100862) and CCEM-CH.

References

[1] G.W. Gibbs, Elementary Principles of Statistical Mechanics, Dover, 1960.
[2] E.T. Jaynes, Information theory and statistical mechanics, Stat. Phys., Brandeis Lect. 3 (1963) 160185.
[3] A.M. Kogan, L.I. Rozonoer, On the macroscopic description of kinetic processes, Dokl. AN SSSR 158 (3) (1964) 566569.
[4] A.M. Kogan, Derivation of Grad-type equations and study of their properties by the method of entropy maximization, Prikl. Math. Mech. 29 (1) (1965) 122133.
[5] R.T. Rockafellar, Convex Analysis, Paperback edition, 1996.
[6] A.N. Gorban, Equilibrium Encircling. Equations of Chemical Kinetics and Their Thermodynamic Analysis, Nauka, Novosibirsk, 1984.
[7] P. Ilg, I.V. Karlin, H.C. Öttinger, Canonical distribution functions in polymer dynamics. (I). Dilute solutions of flexible polymers, Physica A 315 (2002) 367–385.
[8] A.N. Gorban, P.A. Gorban, I.V. Karlin, Legendre integrators, post-processing and quasiequilibrium, J. Non-Newton Fluid Mech. 120 (2004) 149–167.
[9] A.N. Gorban, I.V. Karlin, Method of invariant manifold for chemical kinetics, Chem. Eng. Sci. 58 (2003) 4751–4768.
[10] E. Chiavazzo, A.N. Gorban, I.V. Karlin, Comparison of invariant manifolds for model reduction in chemical kinetics, Commun. Comput. Physics 2 (5) (2007) 964–992.
[11] A.N. Gorban, I.V. Karlin, A.Y. Zinovyev, Invariant grids for reaction kinetics, Physica A 333 (2004) 106–154.
[12] A.N. Gorban, I.V. Karlin, Invariant Manifolds for Physical and Chemical Kinetics, Lecture Notes Physics, 660, Springer, Berlin Heidelberg, 2005, doi: 10.1007/b98103.
[13] J. Li, Z. Zhao, A. Kazakov, F.L. Dryer, Int. J. Chem. Kinetics 36 (2004) 566–575.
[14] E. Chiavazzo, I.V. Karlin, C.E. Frouzakis, K. Boulouchos, Method of invariant grid for model reduction of hydrogen combustion, 2007, arXiv: 0712.2386.
[16] I.V. Karlin, A. Ferrante, H.C. Öttinger, Perfect entropy functions of the lattice Boltzmann method, Europhys. Lett. 47 (1999) 182–188.
[17] S. Arcidiacono, J. Mantzaras, S. Ansumali, I.V. Karlin, C. Frouzakis, K.B. Boulouchos, Phys. Rev. E 74 (2006) 056707.
[18] A.N. Gorban, I.V. Karlin, Thermodynamic parametrization, Physica A 190 (1992) 393–404.
[19] J.C. Keck, D. Gillespie, Combust. Flame 17 (1971) 237.
[20] S.B. Pope, Gibbs function continuation for the stable computation of chemical equilibrium, Combust. Flame 139 (2004) 222–226.
[21] Q. Tang, S.B. Pope, A more accurate projection in the rate-controlled constrained-equilibrium method for dimension reduction of combustion chemistry, Combust. Theory Model. 8 (2004) 255–279.
[22] D. Hamiroune, P. Bishnu, M. Metghalchi, J.C. Keck, Rate-controlled constrained-equilibrium method using constraint potentials, Combust. Theory Model. 2 (1998) 81–94.

[23] P. Bishnu, D. Hamiroune, M. Metghalchi, Development of constrained equilibrium codes and their applications in nonequilibrium thermodynamics, ASME 123 (2001) 214–220.
[24] W.C. Reynolds, The Element Potential Method For Chemical Equilibrium Analysis: Implementation in the Interactive Program STANJAN, Mechanical Engineering Department, Standford University, Standford, CA, 1986.
[25] U. Maas, S.B. Pope, Simplifying chemical kinetics: intrinsic low-dimensional manifolds in composition space, Combust. Flame 88 (1992) 239–264.
[26] V. Bykov, I. Goldfarb, V. Gol'dshtein, U. Maas, On a modified version of ILDM approach: asymptotic analysis based on integral manifolds, IMA J. Appl. Math. (2005) 1–24.
[27] S.H. Lam, D.A. Goussis, Conventional asymptotic and computational singular perturbation for simplified kinetics modelling, in: M.O. Smooke (Ed.), Reduced Kinetic Mechanisms and Asymptotic Approximations for Methane–Air Flames, Springer Lecture Notes, Springer, Berlin, 1991, pp. 227–242.
[28] S.H. Lam, D.A. Goussis, The CSP method for simplifying kinetics, Int. J. Chem. Kinetics 26 (1994) 461–486.
[29] D.A. Goussis, M. Valorani, An efficient iterative algorithm for the approximation of the fast and slow dynamics of stiff systems, J. Comput. Phys. 214 (2006) 316–346.
[30] I.G. Kevrekidis, C.W. Gear, J.M. Hyman, P.G. Kevrekidis, O. Runborg, C. Theodoropoulos, Equation-free: coarse-grained multiscale computation enabling microscopic simulators to perform system-level analysis, Commun. Math. Sci. 1 (2003) 715–762.
[31] A.M. Lyapunov, The General Problem of the Stability of Motion, Taylor & Francis, London, 1992.
[32] N. Kazantzis, Singular PDEs and the problem of finding invariant manifolds for nonlinear dynamical systems, Phys. Lett. A 272 (2000) 257–263.
[36] A.N. Gorban, I.V. Karlin, Uniqueness of thermodynamic projector and kinetic basis of molecular individualism, Physica A 336 (3–4) (2004) 391–432.
[39] H.G. Kaper, T.J. Kaper, Asymptotic analysis of two reduction methods for systems of chemical reactions, Physica D 165 (2002) 66–93.
[41] M.R. Roussel, S.J. Fraser, On the geometry of transient relaxation, J. Chem. Phys. 94 (1991) 7106–7110.
[43] S.J. Fraser, The steady state and equilibrium approximations: a geometrical picture, J. Chem. Phys. 88 (1988) 4732–4738.